Geoscience Frontiers 10 (2019) 1255–1284

HOSTED BY

Contents lists available at ScienceDirect

China University of Geosciences (Beijing)

Geoscience Frontiers

journal homepage: www.elsevier.com/locate/gsf

Focus Paper

# Ophiolites of the Central Asian Orogenic Belt: Geochemical and petrological characterization and tectonic settings

Harald Furnes [a,*], Inna Safonova [b,c]

[a] Department of Earth Science, University of Bergen, Allegt. 41, 5007, Bergen, Norway
[b] Sobolev Institute of Geology and Mineralogy, 3 Koptyuga ave., Novosibirsk 630090, Russia
[c] Novosibirsk State University, 1Pirogova St., Novosibirsk 630090, Russia

ARTICLE INFO

*Article history:*
Received 11 September 2018
Received in revised form
17 December 2018
Accepted 19 December 2018
Available online 20 February 2019
Handling Editor: M. Santosh

*Keywords:*
Geochemical classification
Subduction-unrelated units
Subduction-related units
Subduction fingerprint
Intra-plate magmas
Arc erosion

ABSTRACT

We present a compilation of published data (field, petrography, ages and geochemistry) from 73 ophiolitic complexes of the Central Asian Orogenic Belt. The ophiolitic complexes, ranging in age from Neoproterozoic to Triassic, have been geochemically classified as subduction-related and subduction-unrelated categories applying recent, well-established discrimination diagrams. The subduction-unrelated category is further subdivided into Mid-Ocean Ridge type (MOR), a common rift-drift stage and Plume type, and the subduction-related category is subdivided into Backarc (BA), Forearc (FA), Backarc to Forearc (BA-FA) and Volcanic Arc (VA) types. The four subduction-related types define highly different geochemical features, with the BA and FA types defining end members showing subduction influence of 10%–100% and 90%–100% subduction influence, respectively, and the two other types (BA-FA and VA) define values between the two end members. The subduction-related category comprises 79% of the examined ophiolites, of which the BA type ophiolites is by far the dominant group, followed by the BA-FA type, and with FA and VA types as subordinate groups. The Neoproterozoic and Ordovician complexes exhibit the highest, whereas those of Silurian age exhibit the lowest subduction-influence. Of the remaining 21% subduction-unrelated ophiolites, the MOR type dominates. Both the subduction-related and subduction-unrelated types, in particular the latter, are commonly associated with alkaline basalts taken to represent ocean island magmatism. Harzburgite, dunite, gabbro and basalt are the common lithologies in all ophiolite types, whereas the BA-FA, FA and VA types generally contain intermediate to felsic rocks, and in the FA type boninites occur. The subduction-related ophiolites types generally show low metamorphic grade, whereas greenschist, amphibolite and blueschist grades occur in the subduction-unrelated and BA types. The highly different subduction contribution (from 0 to 100% in the MOR and FA, respectively), attest to variable dips of the subducting slab, as well as variable flux of subduction-related elements into the mantle above subducting slabs, from where the ophiolite magmas got their geochemical fingerprints. As most MOR ophiolites get subducted to the deep mantle, the subduction-related ophiolites have become a dominant ophiolitic type on Earth's surface through all times supporting the idea about the early start of Plate Tectonics.



## 1. Introduction

Ophiolites, the on-land-brought fragments of oceanic crust, represent archives for the evolution and destruction of oceanic crust through time, and provide thus crucial information for the understanding of the evolution of orogenic belts formed in place of former oceans (e.g., Maruyama et al., 1996; Dilek, 2006; Kusky et al., 2013; Furnes et al., 2015). The ophiolite concept has expanded from that of mid-ocean ridge generated oceanic crust (e.g., Moores and Vine, 1971; Anonymous, 1972) to subduction-unrelated and subduction-related ophiolites (Dilek and Furnes, 2011, 2014). Based on the geochemical character of the Troodos ophiolite on Cyprus, Miyashiro (1973) was the first one to question the mid-ocean ridge setting for ophiolite generation, and instead suggested an island arc setting, a revolutionary proposal that led on to the later concept of

* Corresponding author.
*E-mail address:* harald.furnes@uib.no (H. Furnes).
Peer-review under responsibility of China University of Geosciences (Beijing).

https://doi.org/10.1016/j.gsf.2018.12.007

suprasubduction (Pearce et al., 1984). Ophiolites may represent a wide variety with respect to lithological construction and geochemical development (e.g., Dilek and Furnes, 2011, 2014; Pearce, 2014; Saccani, 2015). The main ophiolite division distinguishes subduction-unrelated and subduction-related types, and which further, when applying several geochemical discriminant trace element ratios and abundances (Furnes et al., 2014, 2015; Furnes and Dilek, 2017), can be divided into several subtypes. The subtypes further exhibit their own characteristic lithological construction (see Fig. 2 of Dilek and Funes (2014) and Fig. 1 of Furnes and Dilek (2017)).

In this contribution we present a review of numerous magmatic sequences of the Central Asian Orogenic Belt (CAOB) that have been

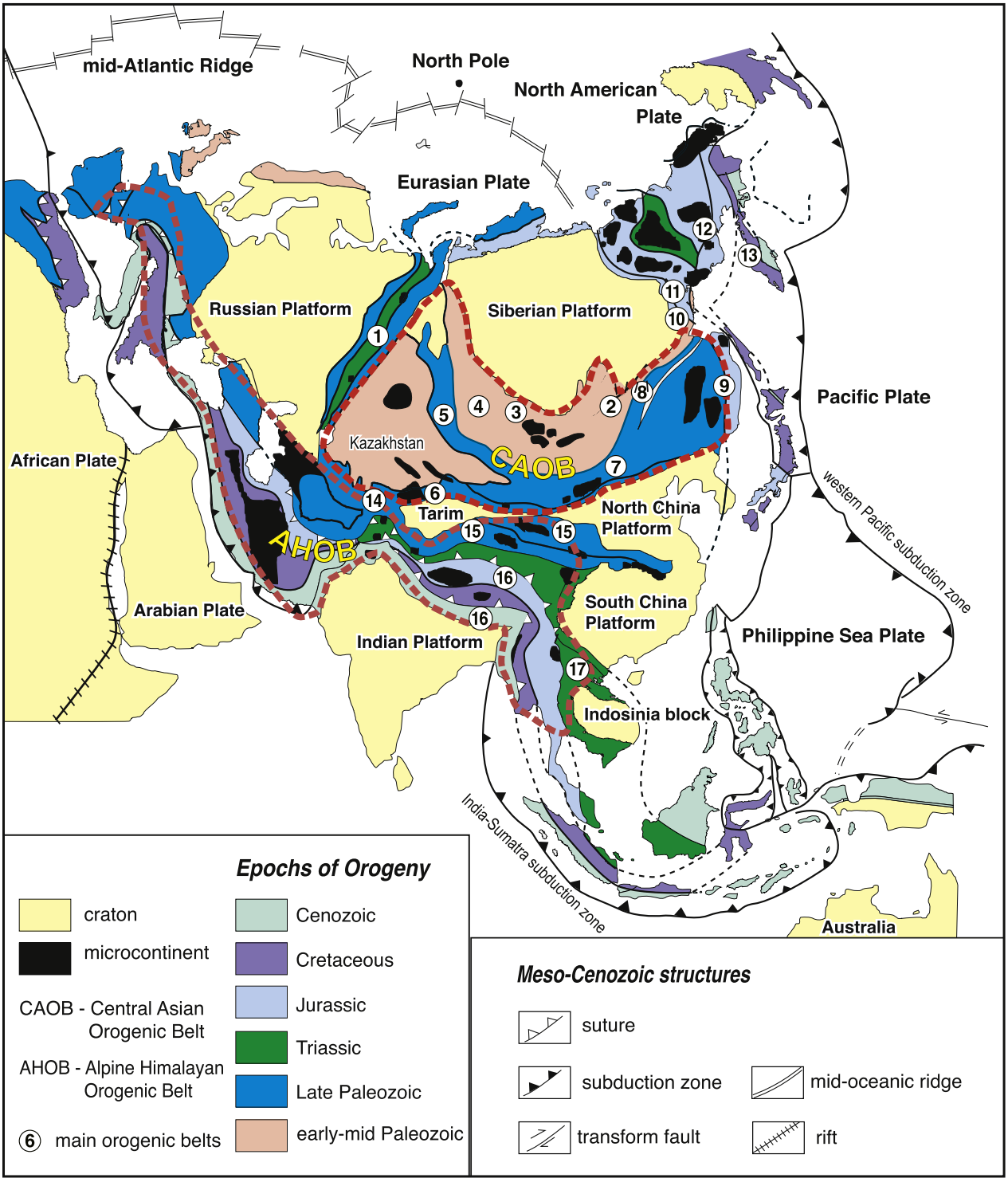


**Figure 1.** General tectonic map of Asia (modified from Maruyama et al., 1989; Safonova and Maruyama, 2014). Numbers in circles are for major orogenic belts: 1 = Uralian, 2–6 = Central Asian (2 = Baikal-Muya, 3 = Yenisey-Transbaikalia-North Mongolia, 4 = Russian-Kazakh-Chinese-Mongolian Altai, 5 = Irtysh-Zaysan, 6 = Kyrgyz-Uzbek-Chinese-Tajik Tienshan), 7 = South-Inner Mongolia, 8 = Mongol-Okhotsk, 9 = Sikhote-Alin, 10 = Verkhoyansk, 11 = Okhotsk-Chukotka, 12 = South Anuy, 13 = West Kamchatka, 14 = Pamir-Hindukush, 15 = Kunlun-Qinling, 16 = Tibet-Himalaya, 17 = South China.

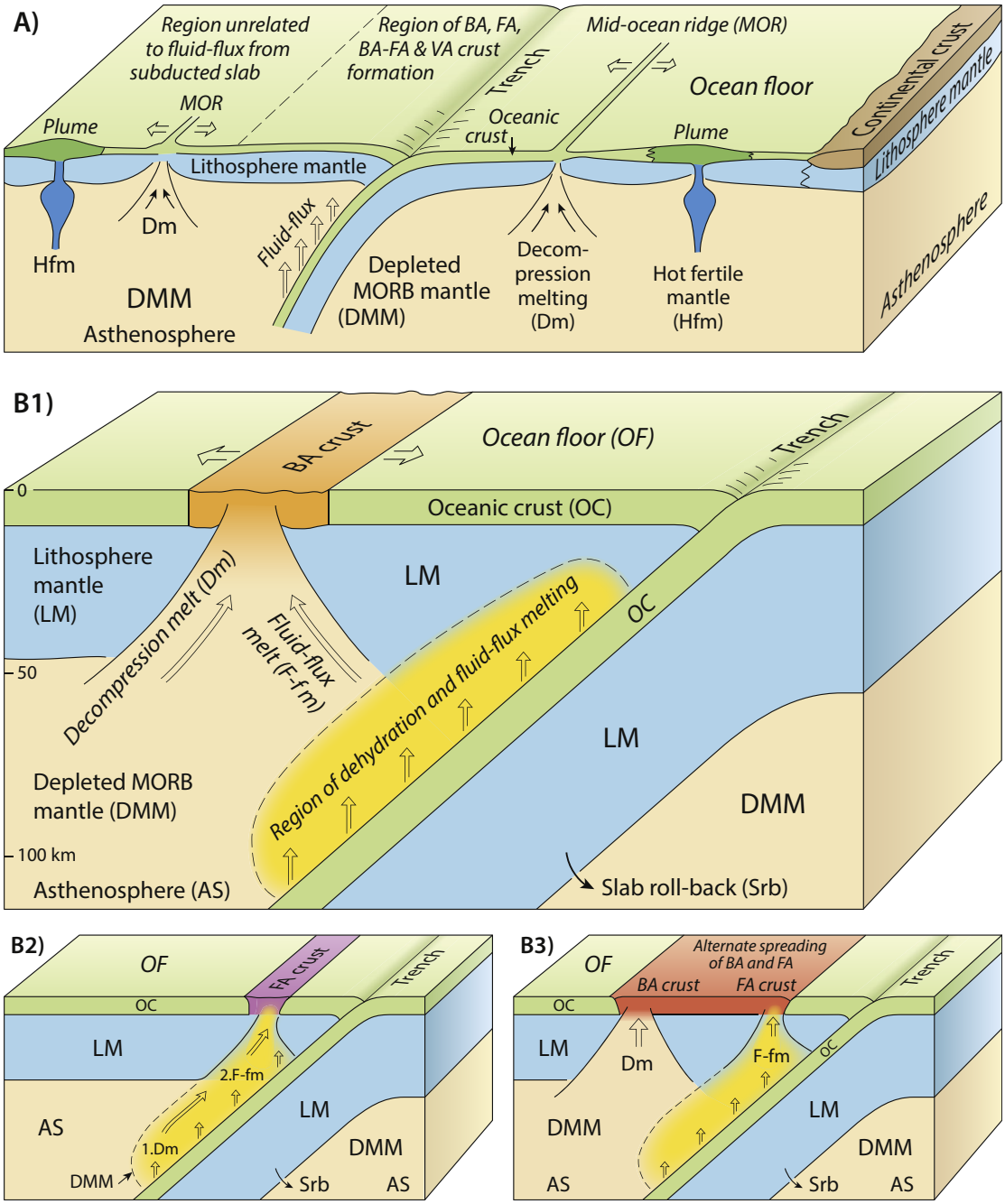


**Figure 2.** Schematic plate tectonic diagrams giving (A) summary of magmatic construction of subduction-unrelated and subduction-related oceanic crust (ophiolites), and (B) details of subduction-related ophiolites, i.e., B1: Backarc (BA), B2: Forearc (FA), B3: Backarc to Forearc (BA–FA). Modified from Pearce (2014) and Furnes and Dilek (2017).

interpreted by many authors as various types of ocean floor construction, i.e., ophiolites and island arcs (see references in Table 1). Some authors, e.g., Sengör et al. (1993, 2018), prefer to us term Altaids, excluding the Neoproterozoic (ca. 1000–600 Ma) rocks, for this huge orogenic belt. Most other scientists ever worked in that region argue for the inclusion of the Neoproterozoic rocks, and use term Central Asian Orogenic Belt (e.g., Zonenshain et al., 1990; Windley et al., 2007; Kröner and Rojas-Agramonte, 2014; Kröner et al., 2014, 2017), the term we use in this paper, and which is briefly described below. We provide general geological and geochemical characteristics of mainly basaltic components such as lavas and dikes (sometimes as sheeted dike complex), as well as isotropic gabbro and apply the geochemical discrimination diagrams of Pearce (2014) and Saccani (2015), in order to classify the numerous complexes (73 in total) of Neoproterozoic to Triassic ages into different ophiolite types as defined by Dilek and Furnes (2011, 2014), Furnes et al. (2014, 2015), Furnes and Dilek (2017).

## 2. The Central Asian Orogenic Belt

The Central Asian Orogenic Belt (CAOB) (Fig. 1) is the world's largest accretionary orogen, formed during the Neoproterozoic to Paleozoic evolution and suturing of the Paleo-Asian Ocean and subsequent collisions of the Siberian, Tarim and North China cratonic blocks, Kazakhstan continent and Precambrian micro-continents (e.g., Zonenshain et al., 1990; Sengor et al., 1993;

**Table 1**
Summary of location, age, and lithology of the investigated complexes.

| Complex/area and abbreviation in parathesis | Location | Age (in Ma or Period) | General geological framework | Lithology | | Metamorphic grade | Main reference(s) |
|---|---|---|---|---|---|---|---|
| | | | | Crustal rocks | Mantle rocks | | |
| **Neoproterozoic** | | | | | | | |
| Eastern Sayan oph. | | | | | | | |
| 1. Dunzhugur (Dr) & | Russia | 1020 | Turbidites on | Gabbro, basalt and boninite | Harz., dun., wehr. | Greenschist | Khain et al. (2002) |
| 2. Ilchir (Il) | Russia–Mongolia | 1020 | top of volcanic rocks | dikes and pillow lava | | Low amphibolite | Sklyarov et al. (2016); Kuzmichev and Larionov (2013) |
| 3. Shishkid (Sd) | Russia–Mongolia | 800 | Shallow to deep-water sediments | Isotropic gabbro, sheeted dikes, basalt and rhyolite | Harz., dun., lhr., wehr. | Low grade | Kuzmichev et al. (2005) |
| 4. Katun 1 (Kt1) | Russia | Late Proterozoic | Oph. mélange | Basalt dikes and pillow lava | | Low grade | Safonova et al. (2011a); Safonova and Santosh, (2014) |
| 5. Kurai (Kr) | Russia | Late Proterozoic | Oph. mélange | Basalt dikes and pillow lava | | Low grade | Safonova and Santosch (2014) |
| 6. Bayankhongor (BH) | Mongolia | 655–636 | Oph. mélange | Gb., basalt dikes and pillow lava | Harz., dun., wehr. | Low grade | Buchan (2001); Jian et al. (2010) |
| 7. Jifeng (Jg) | China (In. M–H) | 647 | Oph. mélange | Gabbro and metabasalt | Ultramafic rocks | Weakly met. | Feng et al. (2016) |
| 8. Gorif (Gf) | Tajikistan | 583–745 | Bedded chert and marble on top of volcanic rocks | Basalt | | Bluesch./gr.schist | Volkova and Budanov (1999) |
| 9. Shatskii (Sk) | Russia | 578 | Oph. mélange | Gabbro, diabase, basalt | Harzburgite | | Mongush et al. (2011) |
| 10. Mayile (Me) | China (Junggar) | 572 | Oph. mélange | Mafic-ultram. cumulate and isotr. gb., massive and pl. lava | Harz., dun., lhz. | Low greenschist | Wang et al. (2003); Yang et al. (2012a) |
| 11. Agardagh Tes-Chem (ATC) | Russia–Mongolia | 570 | Oph. mélange | Gabbro, basalt and bon. dikes, pillow lava, and plagiogranite | Harz., dun., wehr. | | Pfänder et al. (2002) |
| 12 & 13. Khantaishir 1 & 2 (Kh1&2) | Mongolia | 570 | Oph. capped by chert and carb. | Gabbro, basalt and boninite dikes, and pillow lava | Harz., dun. | Low greenschist | Janousek et al. (2018); Gianola et al. (2017) |
| **Cambrian** | | | | | | | |
| 14. Katun 2 (Kt2) | Russia | Early Cambrian | Oph. mélange | Basalt dikes and pillow lava | | Low grade | Safonova et al. (2011a); Safonova and Santosh (2014) |
| 15. Dzhalair-Naiman (DN) | Kazakhstan | E. Camb. 521 Ma | Ophiolite | Gb., bas. dikes, bas., rhyol., pl.gr. | Harz., lhz., wherlite | Low greenschist | Degtyarev (2012) |
| 16. Biluutiin ovoo (Bo) | Mongolia | 525–503 | Oph. mélange | Gb., massive and pl. basalt lava | Serpentinite | | Zhu et al. (2014a) |
| 17. Yueyashan-Xichangjian (YX) | China (Tiansh.) | 533 | Oph. mélange | Cumulate gabbro, massive and pillowed lava | Peridotite | Hydrotherm. alt. | Ao et al. (2012) |
| 18. Hongliuhe (He) | China (Tiansh.) | 520 | Oph. capped by chert, limest. and volcaniclastics | Gabbro, sills, dikes and lava | Harz., lhz., dun. | Low greenschist | Cleven et al. (2015) |
| 19. Chagantaolegai (Cg) | China (Junggar) | 517–519 | Chert | Cum. and isotr. gb., metabas. | Peridotite | Greenschist | Zhao and He (2014) |
| 20. Katun 3 (Kt3) | Russia | Middle Cambrian | Oph. mélange | Basalt dikes and pillow lava | | Low greenschist | Safonova et al. (2011a); Safonova and Santosh (2014) |
| 21. Zoolen (Zl) | Mongolia | 515 | Tect. melange | Gabbro, diorite, basalt, and diabase | Serpentinite | Greenschist | Helo et al. (2006); Jian et al. (2014) |
| 22. Kherlen (Kn) | Mongolia | 500 | Oph. mélange | Gabbro, diabase dikes & basalt | Harz. (serpentinite) | Gr.schist/amph. | Miao et al. (2016) |
| 23. South Hövsgöl (Hl) | Mongolia | 500 | Acc. Prism | Basalt and basaltic andesite | | Greenschist | Medvedev et al. (2008) |
| 24 & 25. Boshchekul | Kazakhstan | L. Camb.–E.Ord. | Volc. sequence ass. w/ granitoids | Gabbro, basalt, andesite, dacite, granodiorite | Serp.; pyroxenite | Amphibolite | Shen et al. (2015); Degtyarev (2012) |
| 26. Chistopol (Cl) | Kazakhstan | Upper Cambrian | Chert ass. w/bas. | Gabbro and basalt | | | Degtyarev et al. (2016) |
| 27. Iradyr (Ir) | Kazakhstan | Upper Cambrian | | Gabbro and basalt | | | Degtyarev et al. (2016) |
| 28. Zasur'ya (Zs) | Russia | Late Cambrian | Oph. mélange | Gabbro, diabase, basalt | | | Safonova et al. (2011b) |
| 29. Selety-Urumbai (Shiil Fm.) (SU) | Kazakhstan | L. Camb.–E. Ord. | Volc. seq.; ass. w/ granitoids | Gabbro, diorite, basalt, bon., and esite, dacite, rhyolite, pl.gr. | | Low grade | Degtyarev (2012) |
| 30. Bingdaban (Bb) | China (Tiansh.) | Early Paleozoic | Oph. mélange | Gabbro, diabase, basalt | | Greenschist | Dong et al. (2007) |
| **Ordovician** | | | | | | | |
| 31. Itmurundy (Iy) | Kazakhstan | Ordovician 445–475 | Oph. mélange<br>Chert and silic.<br>Mudst. on top of<br>Volc. sequence | Gabbro, basalt, AB, andesite | Wehrlite, serp. | Greenschist | Patalakha and Belyi (1981)<br>Kovalenko et al. (1994)<br>unpubl. data of I. Safonova<br>Degtyarev et al. (2016) |

| | | | | | | | |
|---|---|---|---|---|---|---|---|
| 32. Imanburluk (Ik) | Kazakhstan | Lower Ordovician | Chert and silic. mudst. on top of volc. sequence | Gabbro and basalt | | | |
| 33. Aermantai (Ai) | China (Junggar) | 479 | Oph. mélange | Gabbro and basalt lava | Harz., lhz. | | Wang et al. (2003) |
| 34. Tulinkai (Tk) | China (In. M–H) | 438–500 | Oph. mélange | Gabbro and amphibolite | Harz., dun. | Amph./blueschist | Jian et al. (2008) |
| 35. Wudaoshimen (Wn) | China (In. M–H) | 410–500 | | Pillow lava | | Gr.schist/amph. | Song et al. (2015) |
| 36. Kurtushiba (Ka) | Russia | Ordovician | Oph. mélange | Gb., basalt dikes and pillow lava | Harz., dun. | Blusch./gr.schist | Volkova et al. (2009, 2011) |
| 37. Huoshishan-Niujuanzi (HN) | China (Tiansh.) | 435 | Oph. mélange | Gabbro, basalt dikes., andesite and rhyolie volcanics, pl.gr. | Peridotite | Greenschist | Tian et al. (2014) |
| 38. Zhaheba (Zb) | China (Junggar) | 422–495 | Oph. mélange | Gabbro, bas. dikes, bas. pl. lava | Harz., dun. | Hydrotherm. alt. | Luo et al. (2017); Ye et al. (2017) |
| **Silurian** | | | | | | | |
| 39. Alegedayi (Ay) | China (Junggar) | 439 | | Gabbro, bas. dikes, bas. pl. lava | Pyroxenite | Low grade | Wong et al. (2010) |
| 40. Aertengkesi (Ak) | China (Tiansh.) | 423 | Oph. mélange | Gabbro and basalt | Dunite | Low T alteration | Jiang et al. (2014) |
| 41. Serikeyayilake (Se) | China (Tiansh.) | 423 | Oph. mélange | Gabbro and basalt | Harz., lhr. | Low T alteration | Jiang et al. (2014) |
| 42. South Tianshan (ST) | Kyrgyzstan | Late Sil. – Dev. | Oph. mél.(OPS) | Gabbro and basalt | | Low greenschist | Safonova et al. (2016) |
| 43. Edrengiin Nuru (EN) | Mongolia | Mid. Paleozoic | | Basalt and bas.andesite | | Greenschist | Yarmolyuk et al. (2008) |
| **Devonian** | | | | | | | |
| 44. Tseel (Tl) | Mongolia | 397 | | Basalt, dacite, rhyolite | | Greenschist | Demoux et al. (2009) |
| 45. Heiyingshan (Hn) | China (Tiansh.) | 392 | Oph. mélange | Cum. gb., sheeted diab. dikes, massive and pillow basalt | Harz., lhz., dun. | Greenschist | Wang et al. (2011) |
| 46. Dalabute (De) | China (Junggar) | 391 | Oph. mélange | Gabbro, bas.dikes and lava | Serp. peridotite | Sub-greenschist | Liu et al. (2014a) |
| 47. Darbut (Db) | China (Junggar) | 391 | Radiolarian chert | Cumulate gabbro, and basalt pillow lava | Peridotite | Low-T alteration | Wang et al. (2003); Yang et al. (2012b) |
| 48. Baijiantan | China (Junggar) | 385 | Oph. mélange | Gb., bas.dikes and bas. pl. lava | Harz., dun., lhz. | Bluesch./amph. | Zhu et al. (2015) |
| **Baikouquan (BB)** | | | | | | | |
| 49. Sartuohai (Si) | China (Tiansh.) | 368–375 | Oph. mélange | Gabbro and basalt | | Low grade met. | Yang et al. (2012c) |
| 50. Karamaili (Kl) | China (Junggar) | 371 | Red chert and sil. green mudstone | Gabbro, diabase and basalt | Harzburgite | Sub-greenschist | Wang et al. (2003); Liu et al. (2014b) |
| 51. Xinjiang (Xg) | China (Junggar) | Dev. | Tect. Mélange | Gabbro and basalt | | | Niu et al. (2006) |
| 52. East Junggar 1 (EJ1) | China (Junggar) | Devonian | | Mafic to felsic volcanic rocks | | Low grade | Zhang et al. (2009) |
| 53. Nyrnin-Sagan Gp (NS) | Russia | Dev./E.Carb. | | Basalt, andesite and rhyolite | | | Kruk et al. (2008) |
| 54–56. Char (Ch1-3) | E. Kazakhstan | L. Dev./E.Carb. | Oph. mél. (OPS) | Gabbro and basalt | Serpentinite | Low greenschist | Safonova et al. (2012) |
| | E. Kazakhstan | 413–387 | Oph. mélange | Gabbro and basalt | | | Kurganskaya et al. (2014) Safonova et al. (2018a,b) |
| **Carboniferous** | | | | | | | |
| 57. East Junggar 2 (EJ2) | China (Junggar) | Carboniferous | | Basalt and basaltic andesite | | Low grade | Zhang et al. (2009) |
| 58. Xi-Ujimqi (XU) | China (In. M–H) | 331 and 358 | Chert ass. w/pl. | Cum. gb., massive and pl. basalt | | Gr.schist/amph. | Song et al. (2015) |
| 59. Xiaohuangshan (Xn) | China (Tiansh.) | 336 and 345 | Oph. mélange | Gabbro and basalt | Harz., dunite | Med.-high-P met. | Zheng et al. (2013) |
| 60. Guluogou (Gn) | China (Tiansh.) | 334 | Oph. mélange | Gabbro and basalt | Harzburgite | Low-T alteration | Jiang et al. (2014) |
| 61. Khuhu Davaa (KD) | Mongolia | 321–314 | Oph. mélange | Gabbro and basalt | Peridotite | Gr.schist/amph. | Zhu et al. (2017) |
| 62. Shaquanzi (Sq) | China (Tiansh.) | 315–298 | Carbonates and clastic sed. | Basalt, andesite and rhyolite | | Low grade met. | Jiang et al. (2017) |
| 63. Yuejinshan (Ye) | China (In. M–H) | 311 | Oph. mélange | Gabbro and metabasalt | Dun., wherlite | Lower gr,schist | Zhou et al. (2014) |
| 64. Diyanmiao (Do) | China (In. M–H) | 305 | | Cumulate gabbro and pl. lava | Peridotitte | Gr.schist/amph. | Song et al. (2015) |
| 65. Eastern Erenhot (Eh) | China (In. M–H) | 245–353 | Oph. mélange | Gabbro and basaltic dikes | Serp. ult. rocks | Ass. blueschist | Zhang et al. (2015) |
| **Permian** | | | | | | | |
| 66. Daqing Pasture (DP) | China (In. M–H) | 298 | | Gabbro, sheeted dikes, pl.lava | | Gr.schist/amph. | Song et al. (2015) |
| 67. Hegenshan (Hs) | China (In. M–H) | 295–298 | Chert and limest. | Bas.dike compl., massive lava | Harz., lhz., & dunite | Ass. Blueschist | Miao et al. (2008) |
| 68. Liuyuan (La) | China (Tiansh.) | 286 | | Gabbro, massive and pillow lava | Ultramafic rocks | Greenschist | Mao et al. (2012) |
| 69. Dongfanghong (Dg) | China (In. M–H) | 275 | Oph. mélange | Gabbro | | | Sun et al. (2015) |
| 70. Solonker (Sk) | China (In. M–H) | 259 and 263 | Sst. on top of volc | Isotr.gb., rare dikes and bas.lava | Serp. peridotite | Greenschist | Luo et al. (2016) |
| 71. Heilongjiang North (H1) | China (In. M–H) | 258 | Oph. mélange | Metabasalt | | Blueschist | Zhou et al. (2009) |
| 72. Kuznetsk Basin (KB) | Russia | 252–246 | | Basalt, basaltic andesite, trahybasalt lavas and intrusions | | | Nastavko et al. (2012) |
| 73. Manlay (My) | Mongolia | 252–246 | Tuffaceous sst. and mélange | Gabbro, basalt and plagiogranite | Harz. dun. | Weak to moderate alteration | Zhu et al. (2014b) |

(*continued on next page*)

**Table 1** (*continued*)

| Complex/area and abbreviation in parathesis | Location | Age (in Ma or Period) | General geological framework | Lithology | | Metamorphic grade | Main reference(s) |
|---|---|---|---|---|---|---|---|
| | | | | Crustal rocks | Mantle rocks | | |
| **Triassic** | | | | | | | |
| 74. Aluchin (An) | Russia | 226 | Tectoinic contact to adjacent rocks | Gabbro, basalt dikes and lava | Harz. (serpt.), dun. | Low grade | Ganelin (2011) |
| 75. Heilongjiang South (H2) | China (In. M–H) | 220 | Oph. mélange | Metabasalt | | Blueschist | Zhou et al. (2009) |
| 76. Raohe (Re) | China (In. M–H) | 216 | Oph. mélange | Gabbro, dol.dikes and pl.basalt | Peridotite | Low greenschist | Zhou et al. (2014) |

Dobretsov et al., 2003; Windley et al., 2007). The CAOB is believed to be a major site of Phanerozoic juvenile crustal growth (e.g., Jahn, 2004; Safonova, 2017). The formation of CAOB started from the Neoproterozoic accretion of intra-oceanic arcs to the southern margin of the Siberian Craton (e.g., Buslov et al., 2001; Turkina, 2002; Kuzmichev et al., 2005; Safonova et al., 2017). During the rest of the Phanerozoic, many oceanic, island arc, and continental arc terranes as well as microcontinents formerly parts of Gondwanaland were accreted to the southern and western active margins of the Siberian Craton and eastern and southern margins of the Kazakhstan continent (e.g., Kovalenko et al., 2004; Xiao et al., 2010; Donskaya et al., 2013). The late Neoproterozoic to early Paleozoic accretions of arcs and collisions of the Tuva-Mongol, Dzabkhan, Tarbagatai and South Gobi microcontinents with the Siberian Craton formed the central part of CAOB (e.g., Didenko et al., 1994; Salnikova et al., 2001; Kozakov et al., 2007). The western part of CAOB was formed during the Middle Paleozoic collision of the Kazakhstan continent with the Siberian active continental margin. This produced the Altai orogen extended from Russia across eastern Kazakhstan and China to Mongolia (e.g., Buslov et al., 2001; Xiao et al., 2010; Safonova, 2014). Middle to late Paleozoic collisions between the Kazakhstan continent, Tarim Craton and smaller microcontinents formed the Tienshan orogenic belt (e.g., Gao et al., 1998; Biske and Seltmann, 2010; Wang et al., 2010). In Late Permian–Triassic Period the North China Craton approached the island-arc terranes and microcontinents at the southern margin of the Siberian Cratons and the final collision of these two giant cratons formed the eastern part of CAOB (e.g., Zhao et al., 2013; Zhou and Wilde, 2013). All those episodes of collisions between the Siberian, Tarim, and North China cratons and the Kazakhstan continent formed CAOB major orogenic belts (older to younger): Baikal–Muya, Yenisey–Sayan–Transbaikalia–North Mongolia, Russian-Kazakh-Chinese–Mongolian Altai, Irtysh-Zaysan, Kyrgyz-Uzbek-Chinese-Tajik Tienshan, South–Inner Mongolia, Mongol–Okhotsk, and Sikhote–Alin (2–8 in Fig. 1).

## 3. Classification of ophiolites

As shown by Dilek and Furnes (2011, 2014), Kusky et al. (2011, 2013), Pearce (2014), and Furnes and Dilek (2017), ophiolites may be classified according to their geochemical, lithological and structural features. An initial stage in the formation of oceanic crust is represented by the Rift and the Continental Margin types, which by further crustal extension, develops into the Mid-Ocean Ridge type, characterized by a well-organized structural build-up of a lower crustal section of ultramafic cumulates resting on the peridotites of the upper mantle (mainly harzburgites and dunites), and an upper crustal section of gabbro, sheeted dike complex and pillow lavas/massive lavas. A special case of ophiolite development is represented by the Plume type, of which Iceland (North Atlantic) represents an example. This type has a much thicker pile of basaltic volcanic rocks than the other above-mentioned types. In the geochemical compilation of the data we treat the Rift, Continental Margin, and Plume type as one group, subsequently referred to as the R/CM/P type, and the Mid-Ocean Ridge type as MOR type (Fig. 2A). This is rather similar to the classification of Kusky et al. (2011, 2013) in which our MOR type corresponds to their Fast Penrose and Slow Hess types, formed during fast and slow spreading, respectively. Further, their Hotspot Oceanic Plateau, corresponds to our Plume type, and their Transitional Tihama Asir type, developed at stretched continental margin, correspond to a transition between our Rift and Continental Margin types. The ophiolite complexes that develop in the subduction-related tectonic environment, or commonly referred to as supra-subduction zone (SSZ) environment, are generally more complex than the

above-mentioned types. These ophiolite types may vary from the relatively simple type, i.e., the Backarc type, to the more complex and lithologically diverse Forearc, the Backarc to Forearc, and Volcanic Arc types, referred to below as BA, FA, BA-FA, and VA types, respectively (Fig. 2B1–B3). Our VA type (see description below) corresponds to the Intra-arc Smartville type of Kusky et al. (2011, 2013), and for the present compilation the distinction between the subduction-related complexes are based mainly on the geochemical character described below.

The Backarc type may structurally look like MOR-generated oceanic lithosphere, but their crustal and upper mantle units may have different geochemical fingerprints. Forearc oceanic crust may share structurally and lithologically similarities with that of the MOR oceanic crust (particularly in its lower sections), but differs from the subduction-unrelated ophiolites in its upper crustal sections, by the presence of intermediate (andesitic) to silicic (dacite and rhyolite) extrusive and intrusive rocks, and with boninitic extrusive and intrusive rocks (Dilek and Thy, 2009). The Backarc to Forearc oceanic crust makes up a hybrid type between that of Backarc- and Forearc-generated oceanic crust. The Volcanic Arc oceanic crust represents a long time of magmatic construction (more than 20–30 million-years) in a suprasubduction zone setting (Dilek et al., 1991; Dilek and Furnes, 2011). The middle to lower crust of this type is dominated by abundant intrusions of diorite, tonalite and granodiorite (see Fig. 1 of Furnes and Dilek, 2017), and thick accumulations of basaltic, dacitic and rhyolitic subaerial volcanic rocks (see Fig. 1 of Furnes and Dilek, 2017). Hence, the thickness of this type maybe considerably larger than the other subduction-related ophiolite types.

During the tectonic emplacement of ophiolites the lithologies of an oceanic plate may be dismembered, some subducted and others accreted. In most cases only the upper parts of the original sequence are typically available for investigation. Thus, it is convenient to use the geochemical characteristic of the basaltic lavas and dikes, as well isotropic gabbro of the ophiolites for the purpose of classification.

During the last four decades a large number of element combinations in basaltic rocks from modern tectonic settings have been employed in order to fingerprint different tectonic environments for old magmatic sequences (e.g., Pearce and Cann, 1971, 1973; Pearce and Norry, 1979; Shervais, 1982; Pearce, 2008, 2014; Saccani, 2015). However, the tectonic fields in most diagrams often overlap thus making their application restricted and requiring a strong control by geological data. The most employed and successful discrimination diagrams though are based on elements Ti, V, Zr, Y, Nb, Th and Yb. As a general consensus, resulting from numerous studies, these seven elements are considered to be stable during post-magmatic alteration and metamorphism of basaltic rocks (e.g., Scott and Hajash, 1976; Staudigel and Hart, 1983; Seyfried et al., 1988; Komiya et al., 2004; Hofmann and Wilson, 2007; Dilek et al., 2008; Furnes et al., 2012). Combinations of these elements, as outlined below, thus provide a good proxy for reconstructing the composition of the original magma.

For geochemical classification of ophiolitic basalts, and, to a lesser extent, basaltic andesites, we have used combinations of the above-mentioned seven elements in four discrimination diagrams: Zr/Ti–Nb/Y, Th/Yb–Nb/Yb, V–Ti/1000, and $TiO_2$/Yb–Nb/Yb. The classification involves four steps (Fig. 3), following the method of Pearce (2014). As the first step, we have used the Zr/Ti–Nb/Y diagram of Floyd and Winchester (1975) in order to select only data from rocks of basaltic composition. For non-metamorphosed rocks this step would not have been necessary, since the $SiO_2$ and MgO contents would classify the rock as basalt. However, both Si and Mg are unstable and mobile elements during hydrothermal alteration and metamorphism, and thus unreliable for the use of classification. Thus, since all ophiolite complexes have undergone alteration and/or metamorphism, stable elements (like Ti, Y, Zr, Nb) are employed for a safe classification. The second step employed the Th/Yb–Nb/Yb diagram of Pearce (2008) to discriminate subduction-related and subduction-unrelated basalts. All basalts that plot within the OIB-MORB array (also known as the mantle array) have been considered as unrelated to subduction, whereas those plotting above it are interpreted to be influenced by subduction, yielding Th-enriched fluids released from the subducting slab during subduction. The subduction-related basalts encompass oceanic and continental arc types, or plot within the area between the mantle array and the arc type fields. Step 3 involves further discrimination of the basalts using the V/Ti ratio as a proxy for supra-subduction zone (SSZ) derivation (Shervais, 1982). The modified V–Ti diagram (Pearce, 2014) discriminates between boninite, island-arc tholeiite (IAT), and MORB fields, the latter and former representing the tectonic environment most distant and nearest from a trench and the associated subduction zone, respectively. Basalts that plot within the OIB-MORB array of the Th/Yb–Nb/Yb diagram have been further analyzed in the $TiO_2$/Yb–Nb/Yb diagram (Step 4), as the $TiO_2$/Yb ratio is a good indicator of the depth of mantle melting (Pearce, 2014). During shallow melting of spinel peridotites Ti and Yb are similarly partitioned in the melt, whereas for deep melting of garnet peridotites these two elements are decoupled, since Yb is strongly partitioned in garnet, but not in spinel. Thus, the retention of Yb in residual garnet, but not in residual spinel, results in deep- and shallow-generated melts, respectively, with high Ti/Yb ratio at depth where garnet is stable, and melts of low Ti/Yb in the absence of garnet (Hirschman and Stolper, 1996).

Following this classification scheme, ophiolitic basalts are first divided into two main groups: subduction-unrelated and subduction-related (Dilek and Furnes, 2011, 2014). The subduction-unrelated group can be further discriminated into Rift/Continental Margin, MOR, and Plume types, a subdivision that is defined by their grouping in the $TiO_2$/Yb–Nb/Yb diagram. MOR type basalts plot within the MORB array while plume-related basalts plot within the OIB array and the Rift/Continental Margin types fall into the alkaline field of the OIB array (Fig. 3). The subduction-related basalts can be subdivided into BA, BA-FA, FA, and VA types. The BA, BA-FA, and FA types are recognized as such when the majority of their compositions plot in the oceanic arc (as well as joint oceanic arc/continental arc) field of the Th/Yb–Nb/Yb diagram (Fig. 3, step 2) and in the MORB, IAT and boninite fields in the V–Ti diagram (Fig. 3, step 3), respectively. For the samples that we classify as VA basalts the data plot mainly in the continental arc field of the Th/Yb–Nb/Yb diagram and within the IAT and boninite fields in the V–Ti diagram. Admittedly, in some cases it is difficult to assign a specific tectonic environment for a complex when there is a large spread in the data points, and also, when the number of data points is low. Preferably petrographic and field-related data-control, together with the geochemical characteristics would have been preferred. To some limited extent the description of the crustal lithology (Table 1) give some control, i.e., that the complexes assigned as BA-FA and FA types show a wider spread in the rock composition than those classified as BA type (more comprehensively dealt with in Chapter 6). However, in many cases, only a fraction of the anticipated total original rock components are available for study, and in such cases only the geochemical fingerprints of the basaltic rocks are available for classification. Thus, the classification of the complexes into different ophiolite types is in this study mainly based on their geochemical characteristics.

Another new discrimination diagram is provided by the MORB-normalized values of Th and Nb (Saccani, 2015). This diagram (Fig. 4) is useful in combination with the discrimination diagrams

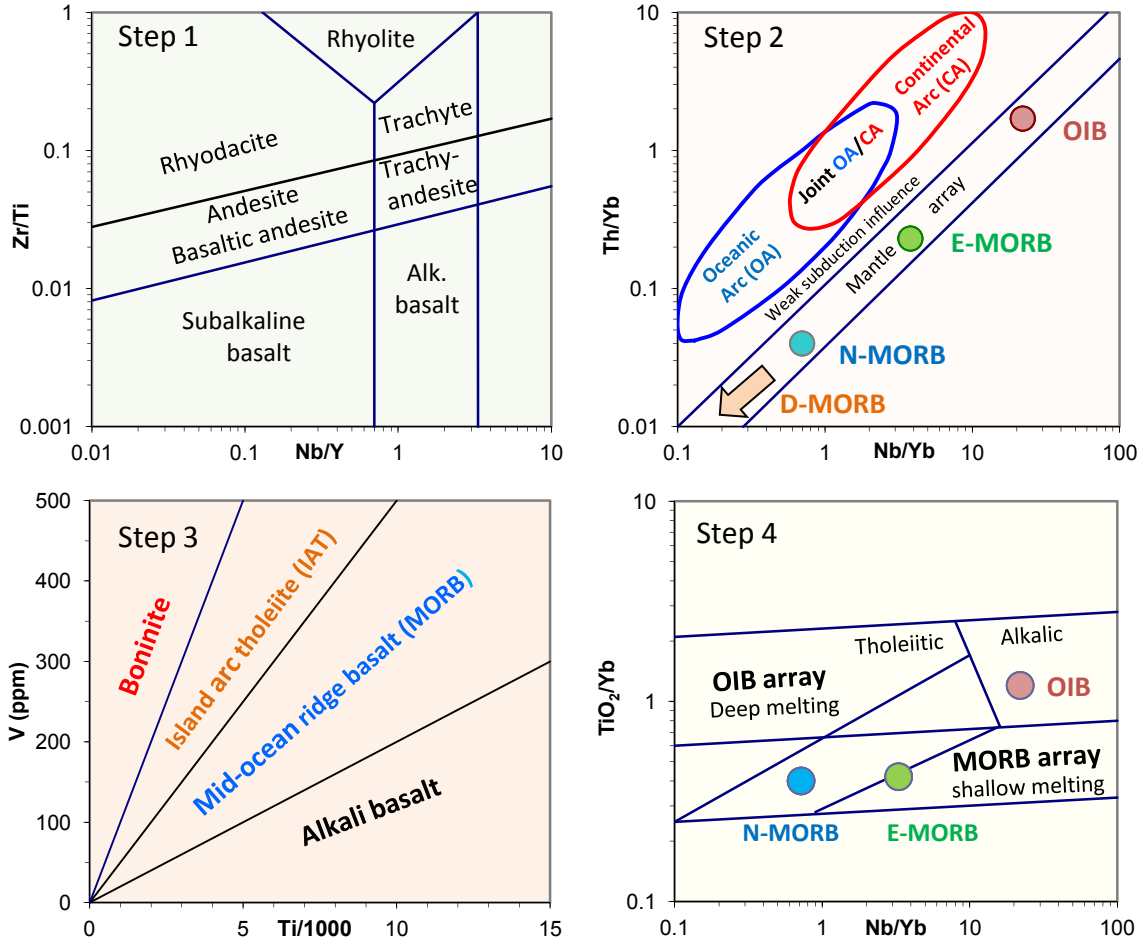


**Figure 3.** Templates for various discrimination diagrams used for the geochemical classification and discrimination of tectonic settings of formation of ophiolitic crustal units (after Pearce, 2014). The Zr/Ti– Nb/Y diagram (step 1) is originally after Floyd and Winchester (1975), the Th/Yb–Nb/Yb (step 2) and $TiO_2$/Yb–Nb/Yb (step 4) diagrams after Pearce (2008), and the V–Ti/1000 (step 3) diagrams after Shervais (1982), and modified by Pearce (2014).

shown in Fig. 3. In this discrimination diagram, like most others, there are overlaps between the fields of different environments. But, important is the distinction between basalts of subduction-related and subduction-unrelated backarc basins. About half of the backarc field overlaps largely with those of N-MORB and E-MORB without subduction influence. This is important to keep in mind when classifying ophiolites, implying that those classified as MOR-type (N-MORB and E-MORB) may be part of a backarc system (e.g., Zhang et al., 2018a, b). In fact, this is well demonstrated for the active backarc East Scotia Ridge (South Atlantic Ocean), of which some of the spreading segments show basalt derivation from unmodified MORB mantle, and others are subduction-modified (Fretzdorff et al., 2002).

## 4. Geological and petrological summary of the investigated complexes

A total of seventy-three ophiolitic and/or island arc complexes of the CAOB have been included in the present review. These include complexes from Russia (11), Kazakhstan (9), Mongolia (13), China (38), Tajikistan (1) and Kyrgyzstan (1). Their distribution within the CAOB, color-coded with respect to age, is shown in Fig. 5. A short summary of the mantle and crustal lithologies, the metamorphic conditions, tectonic framework, and main reference(s) to each of the complexes is given in Table 1. Mantle lithologies have been reported from forty-four of the complexes. The most common ultramafic rock is harzburgite, but also lherzolite, dunite, wehrlite, and pyroxenite are reported (Table 1). In some of the complexes the ultramafic rocks are only categorized as serpentinized peridotite, due to pervasive alteration. Of the lower crustal part of the

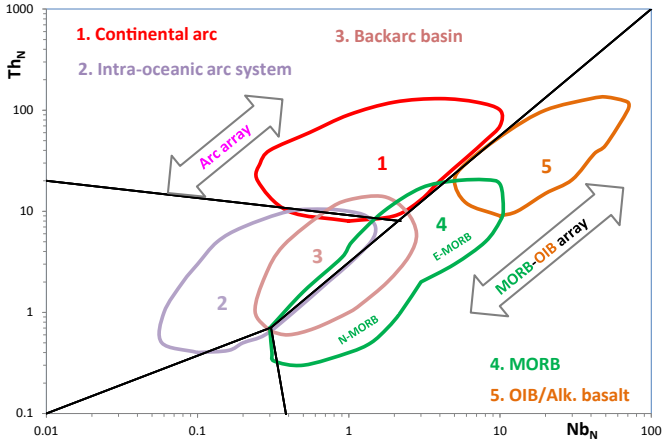


**Figure 4.** Template for the $Th_N$–$Nb_N$ discrimination diagram. Modified and simplified after Saccani (2015).

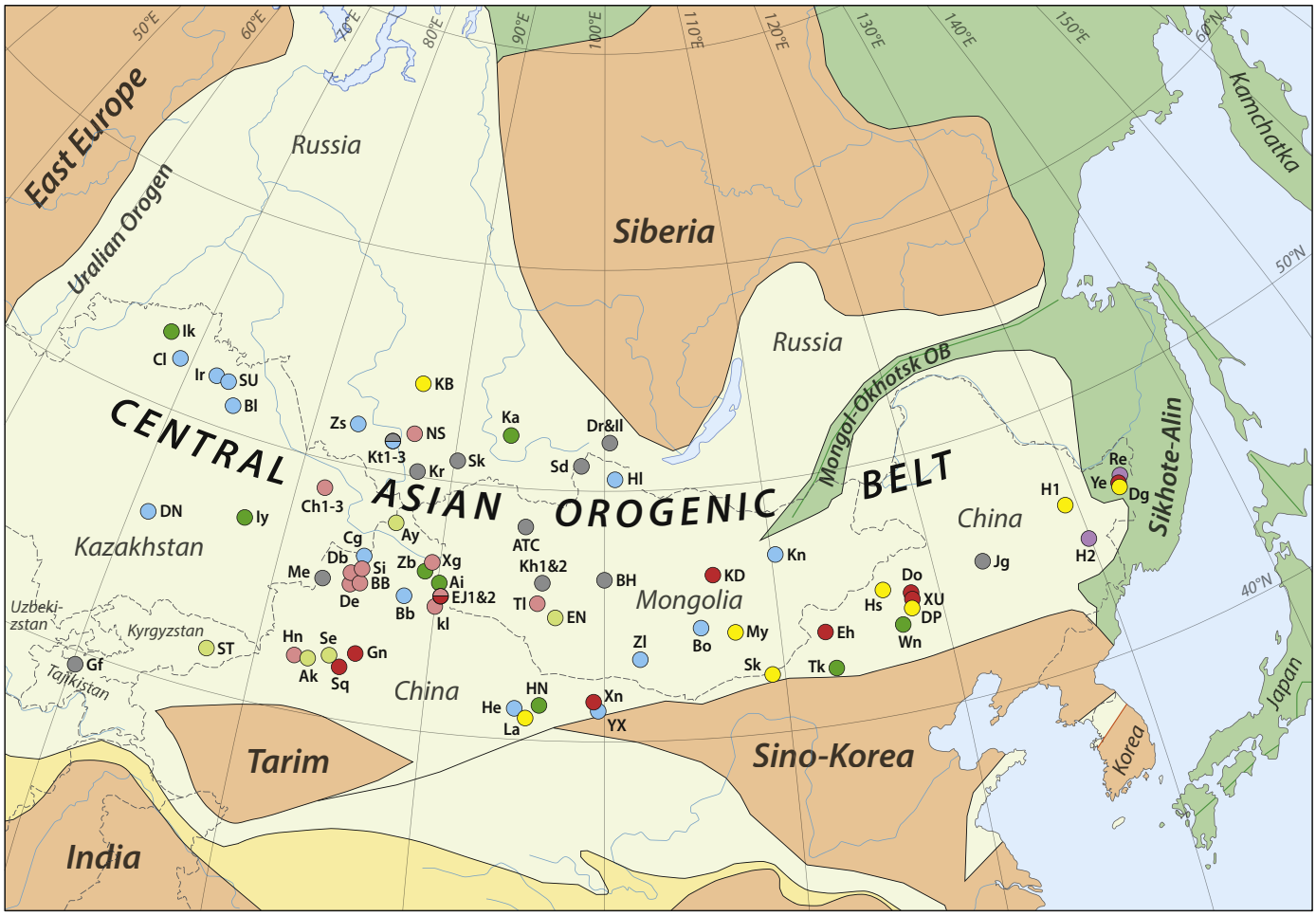


**Neoproterozoic**
Dunzhugur (Dr)
Ilchir (Il)
Shishkid (Sd)
Katun 1 (Kt1)
Kurai (Kr)
Bayankhongor (BH)
Jifeng (Jg)
Gorif (Gf)
Shatskii (Sk)
Mayile (Me)
Agardagh Tes-Chem (ATC)
Khantaishir1&2 (Kh1&2)

**Cambrian**
Katun 2 (Kt2)
Dzhalair-Naiman (DN)
Biluutiin ovoo (Bo)
Yueyashan-Xichangjian (YX)
Hongliuhe (He)
Chagantaolegai (Cg)
Katun 3 (Kt3)
Zoolen (Zl)
Kherlen (Kn)
S. Hövsgöl (Hl)
Boshchekul (Bl)
Chistopol (Cl)
Iradyr (Ir)
Zasur'ya (Zs)
Selety-Urumbai (Shiil Fm.) (SU)
Bingdaban (Bb)

**Ordovician**
Itmurundy (Iy)
Imanburluk (Ik)
Aermantai (Ai)
Tulinkai (Tk)
Wudaoshimen (Wn)
Kurtushiba (Ka)
Huoshishan-Niujuanzi (HN)
Zhaheba (Zb)

**Silurian**
Alegedayi (Ay)
Aertengkesi (Ak)
Serikeyayilake (Se)
S. Tianshan (ST)
Edrengiin Nuru (EN)

**Devonian**
Tseel (Tl)
Heiyingshan (Hn)
Dalabute (De)
Darbut (Db)
Baijiantan-Baikouquan (BB)
Sartuohai (Si)
Karamaili (kl)
Xinjiang (Xg)
E. Junggar 1 (EJ1)
Nyrnin-Sagan Gp (NS)
Char (Ch1-3)

**Carboniferous**
E. Junggar 2 (EJ2)
Xi-Ujimqi (XU)
Xiaohuangshan (Xn)
Guluoegn (Gn)
Khuhu Davaa (KD)
Shaquanzi (Sq)
Yuejinshan (Ye)
Diyanmiao (Do)
Eastern Erenhot (Eh)
Char (Ch2)

**Permian**
Daqing Pasture (DP)
Hegenshan (Hs)
Liuyuan (La)
Dongfanghong (Dg)
Solonker (Sk)
Heilongjiang North (H1)
Kuznetsk Basin (KB)
Manlay (My)

**Triassic**
Aluchin (An)
Heilongjiang South (H2)
Raohe (Re)

**Figure 5.** Outline of the Central Asian Orogenic Belt (modified from Safonova and Santosh, 2014), showing the geographical position of the Neoproterozoic to Triassic investigated complexes.

complexes, gabbro, basalt dikes (sometimes reported as sheeted dike complex) and basalt lava are reported in fifty-five of the complexes. The basaltic lava (also basaltic andesite and boninite in some of the complexes) is reported as pillow lavas in twenty-three of the complexes, and only as basalt in thirty-one of the complexes. In the latter case this could involve lava (pillow lava) and/or dikes. For a few complexes, i.e., Gorif, Wudaoshimen, Heilongjiang, and Dongfanghong, only basalt and gabbro are reported (Table 1). Felsic igneous rocks, both volcanics and/or intrusives, have been reported in several of the complexes (i.e., Shishkid, Dzhalair-Naiman, Boshchekul, Selety-Urumba (Shiil Fm.), Huoshishan-Niujuanzi, Tseel). The metamorphic grade has been reported from sixty of the complexes (Table 1), and the majority (forty-two) has been reported as low grade, i.e., hydrothermal alteration and greenschist metamorphism. The remaining complexes have been reported to have undergone greenschist-amphibolite-blueschist metamorphic grade (Table 1). The majority of the complexes occur as ophiolitic mélanges, and many of them are capped by pelagic chert, hemipelagic siliceous mud/siltstone, turbidite/greywacke sandstones, limestone and volcaniclastics, i.e., lithological associations recognized as ocean plate stratigraphy, or OPS (Isozaki et al., 1990; Maruyama et al., 2010; Safonova and Santosh, 2014; Safonova et al., 2016; Zhang et al., 2018a,b). Within the numerous subduction-accretion complexes of the CAOB, blueschist and eclogite also occur (e.g., Volkova and Sklyarov, 2007; Windley et al., 2007; Stipska et al., 2010; Liu et al., 2014; Zhao and He, 2014), of

which the protoliths to some of them can be shown to be of MORB and IAT character (Ni et al., 2006; Zhang et al., 2018c).

Altogether, the majority of the investigated complexes of the CAOB exhibit the typical rock association of ophiolites in terms of mantle and crustal lithologies, the metamorphic grade, and tectonic framework (e.g., Dilek and Furnes, 2011, 2014; Furnes and Dilek, 2017; Safonova et al., 2017). Further, the recognition of OPS in most of the complexes (e.g., Maruyama et al., 2010; Kusky et al., 2013; Safonova and Santosh, 2014; Safonova et al., 2016), is also an important part of such complexes in terms of the interpretation of their tectonic setting from the initial deposition of fine-grained sedimentary and volcanic rocks syn-genetically with the formation of the oceanic crust, to the time of getting incorporated in the accretionary prism at a Pacific-type convergent margin (Safonova, 2017).

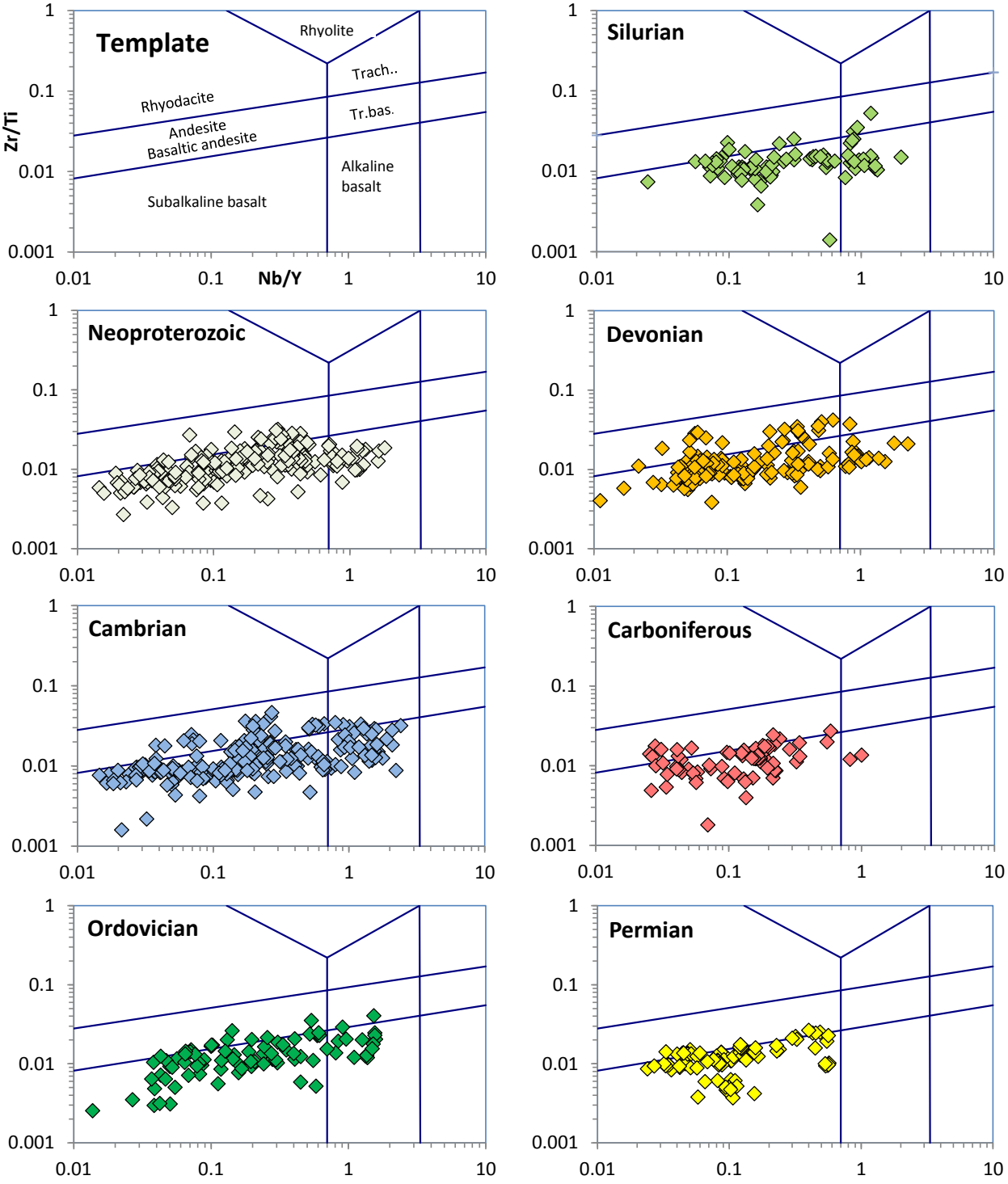


**Figure 6.** Nb/Y–Zr/Ti diagram to distinguish between subalkaline and alkaline basalts (modified after Floyd and Winchester, 1975).

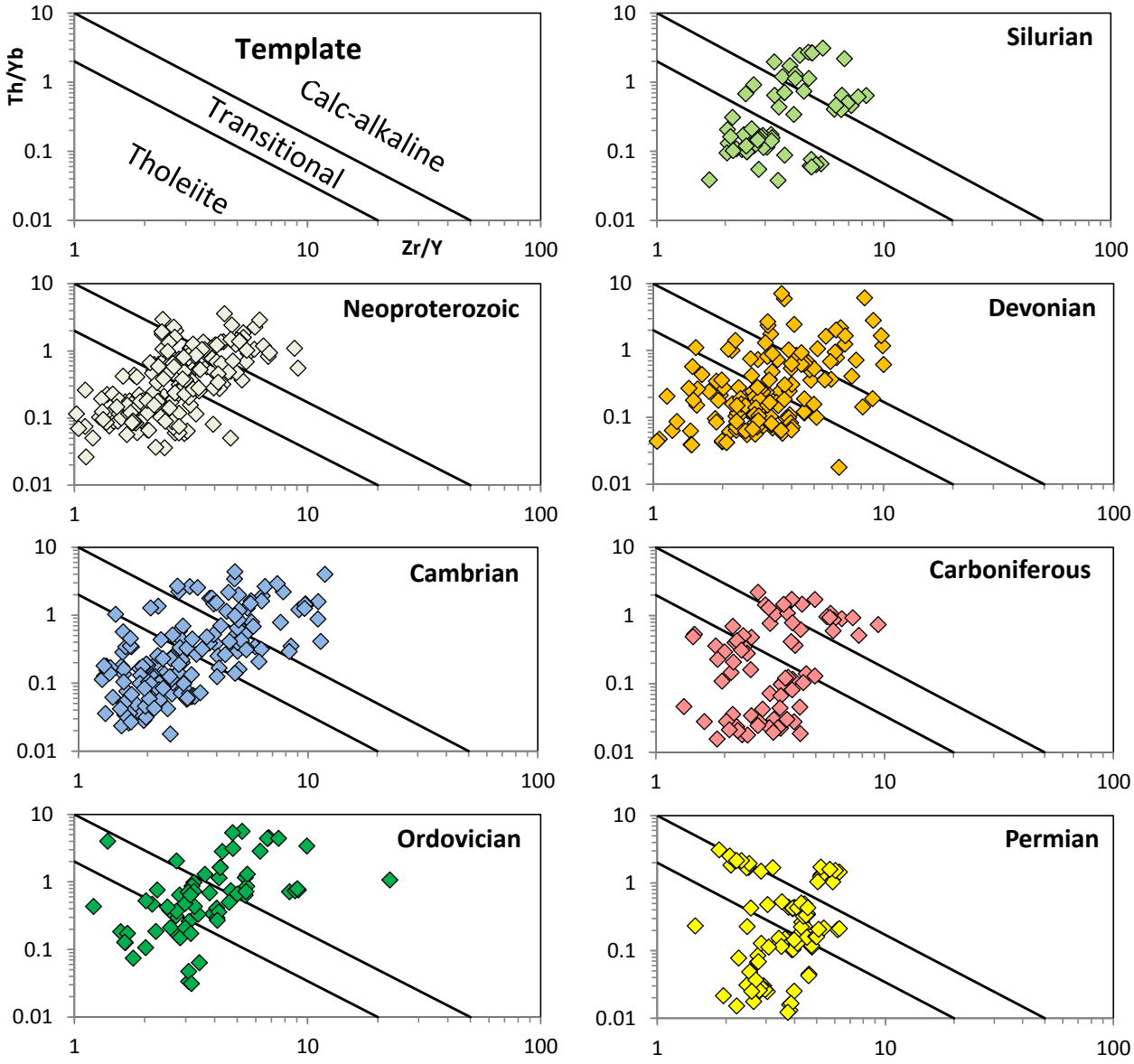


**Figure 7.** Zr/Y–Th/Yb diagram to distinguish between tholeiitic and calc-alkaline basalts (modified after Ross and Bedard, 2009).

## 5. Geochemical characteristics of the investigated complexes

The geochemical data base used for this compilation is based on 85 published papers as well as unpublished data (by I. Safonova), comprising a total of 986 analyses. All of the papers, except one (published in 1999), are 2000-papers. The number of analyses from the various complexes is highly different, but for the majority of the complexes (ca. 60%), each one have ten (or more) analyses available,

**Table 2**
Magmatic character of the basalts of the investigated complexes.

| Age | Number of sequences and analyses in paranthesis | Magmatic affinity (in %) | | | | |
|---|---|---|---|---|---|---|
| | | Alkaline | Subalkaline | Subalkaline division | | |
| | | Nb/Y > 0.7 | Nb/Y < 0.7 | based on Zr/Y vs. Th/Yb character | | |
| | | | | Tholeiite | Transitional | Calc-alkaline |
| Neoproterozoic | 13 (228) | 12 | 88 | 51 | 32 | 17 |
| Cambrian | 17 (208) | 19 | 81 | 54 | 24 | 22 |
| Ordovician | 7 (79) | 19 | 81 | 35 | 30 | 35 |
| Silurian | 5 (85) | 26 | 74 | 57 | 12 | 31 |
| Devonian | 11 (142) | 13 | 87 | 61 | 23 | 16 |
| Carboniferous | 9 (84) | 2 | 98 | 63 | 16 | 21 |
| Permian | 7 (88) | 0 | 100 | 52 | 36 | 12 |
| Triassic | 2 (21) | 52 | 48 | | | |

and ca. 15% has seven (or less) analyses. A weakness that should be pointed out is that the literature-based geochemical data used in the geochemical processing are produced in several different laboratories. A strength, however, of this work is that the data of each sequence has been similarly processed.

### 5.1. Magmatic character

The magmatic character in terms of distinction between alkaline, tholeiitic and calc-alkaline magmatic series has traditionally been based on the alkali–total iron–magnesium (AFM) diagram (Irvine and Baragar, 1971) and the total alkali–silica (TAS) diagram (Le Maitre, 1989). However, most of the investigated basaltic rocks are altered or have suffered greenschist grade metamorphism, and some have been subject of medium- to high-grade metamorphism (Table 1), and classification based on mobile major elements including Na, K, and Mg is therefore unreliable. Instead we use the immobile elements Ti, Zr, Y, Nb, Th and Yb to test the magmatic character. First we employ the Nb/Y–Zr/Ti diagram of Winchester and Floyd, (1977) to distinguish between subalkaline and alkaline basalts (Fig. 6). Then we isolate all the subalkaline basalts and plot those in the Zr/Y–Th/Yb discrimination diagram of Ross and Bedard

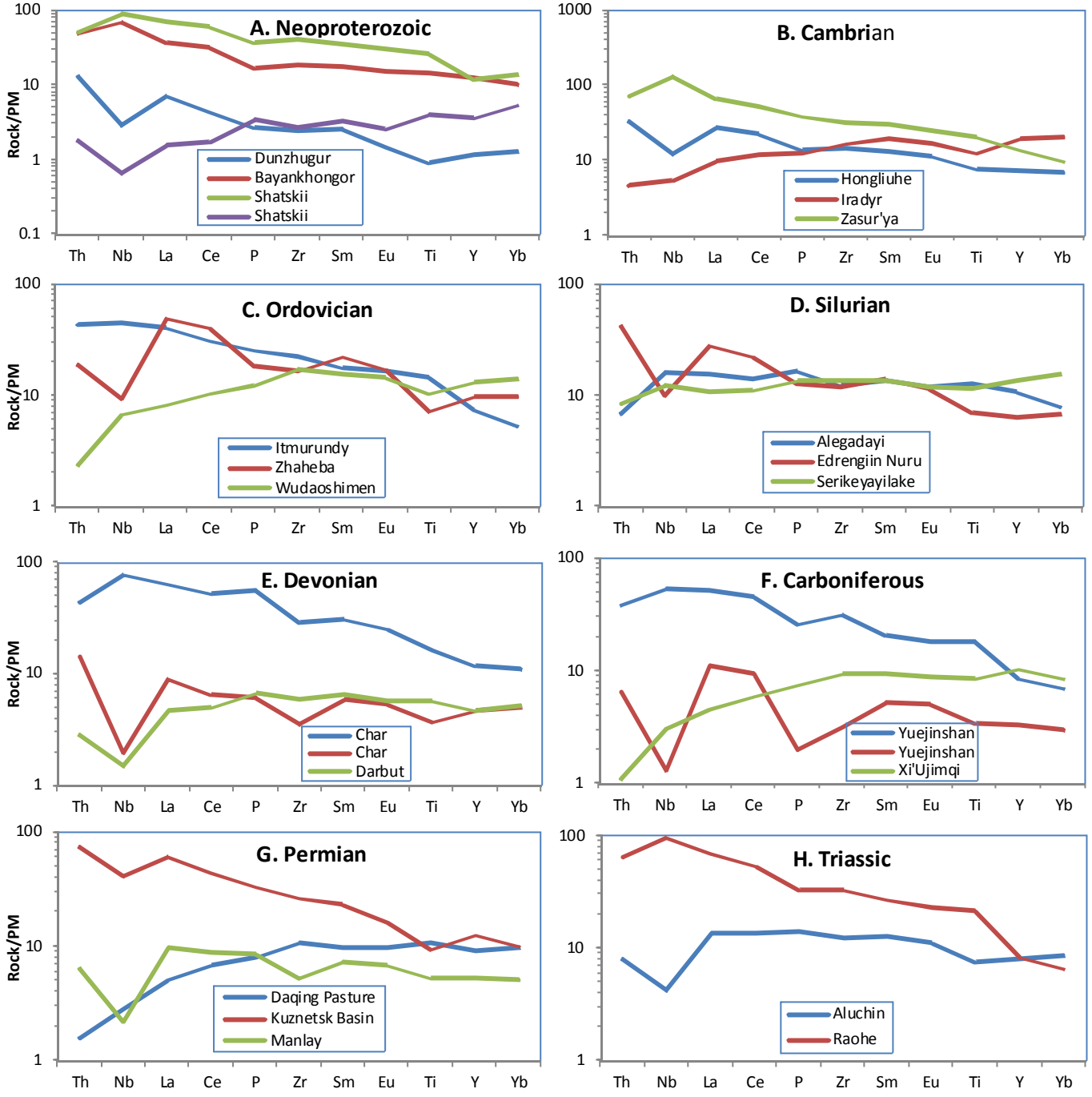


**Figure 8.** Representative PM-normalized multi-element diagram of the Neoproterozoic through Triassic complexes investigated. References to geochemical data are given in Supplementary Table 1. The PM values are from Lyubetskaya and Korenaga (2007): Th: 62.6 ppb; Nb: 460 ppb; La: 508 ppb; Ce: 1340 ppb; P: 66 ppm; Zr: 8.42 ppm; Sm: 324 ppb; Eu: 123 ppb; Ti: 950 ppm; Y: 3.37 ppm; Yb: 346 ppb.

(2009) to distinguish between tholeiitic and calc-alkaline character (Fig. 7). In general, the subalkaline basalts are dominant compared to those of alkaline character, and for the Carboniferous and Permian basalts, only subalkaline basalts occur (Fig. 6). Of the subalkaline basalts, tholeiitic basalts are the dominant type, whereas calc-alkaline basalts in general are subordinate (Fig. 7). The magmatic character of the Neoproterozoic to Triassic basalts is summarized in Table 2. For the Triassic complexes, however, only two examples are included in this study. Hence, in this compilation no general characterization of the magmatic rocks of this age group should be done.

### 5.2. Multi-element character

Representative multi-element diagrams for the basaltic rocks of each of the Neoproterozoic through Triassic ophiolite and island arc complexes of the CAOB, defined as PM (primitive mantle)-normalized values of Th, Nb, La, Ce, P, Zr, Sm, Eu, Ti, Y and Yb (element values from Lyubetskaya and Korenaga, 2007), are shown in Fig. 8. The complete data base for each of the complexes and the multi-element diagrams are presented as Supplementary Figs. 1–8. The eleven chosen elements have been placed in order of increasing compatibility, with Th being the most incompatible and Yb the least incompatible during melting of a spinel-lherzolite mantle (Pearce and Parkinson, 1993).

The Neoproterozoic basaltic sequences in general define a pattern with increasing PM-normalized values towards the most incompatible elements, and most of the complexes show a significant negative Nb-anomaly (Fig. 8A). However, the basalts from some of the complexes, i.e., those of Bayankhongor, Gorif, Mayile, and partly Shatskii, do show a slight positive Nb-anomaly (Fig. 8A). Many of the Cambrian complexes define similar PM-normalized multi-element patterns to those of the Neoproterozoic complexes, i.e., with positive and minor to significant negative Nb-anomalies.

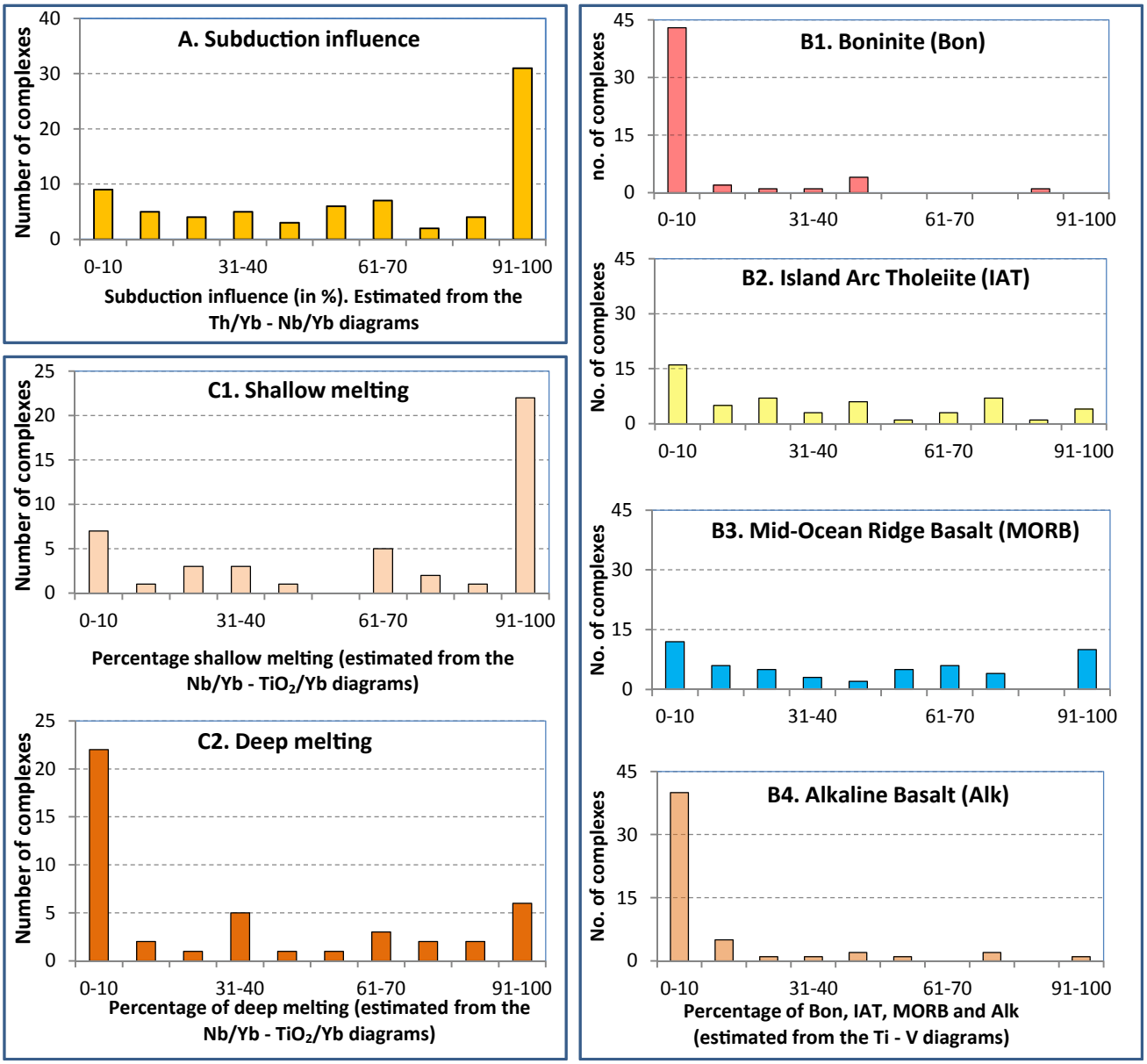


**Figure 9.** Histograms summarizing: (A) the percentage of subduction influence; (B) the proportion (in %) of boninite, IAT, MORB, and alkali basalts of the subduction-influenced basalts; and (C) the melt regime (shallow or deep) of the subduction-unrelated basalts.

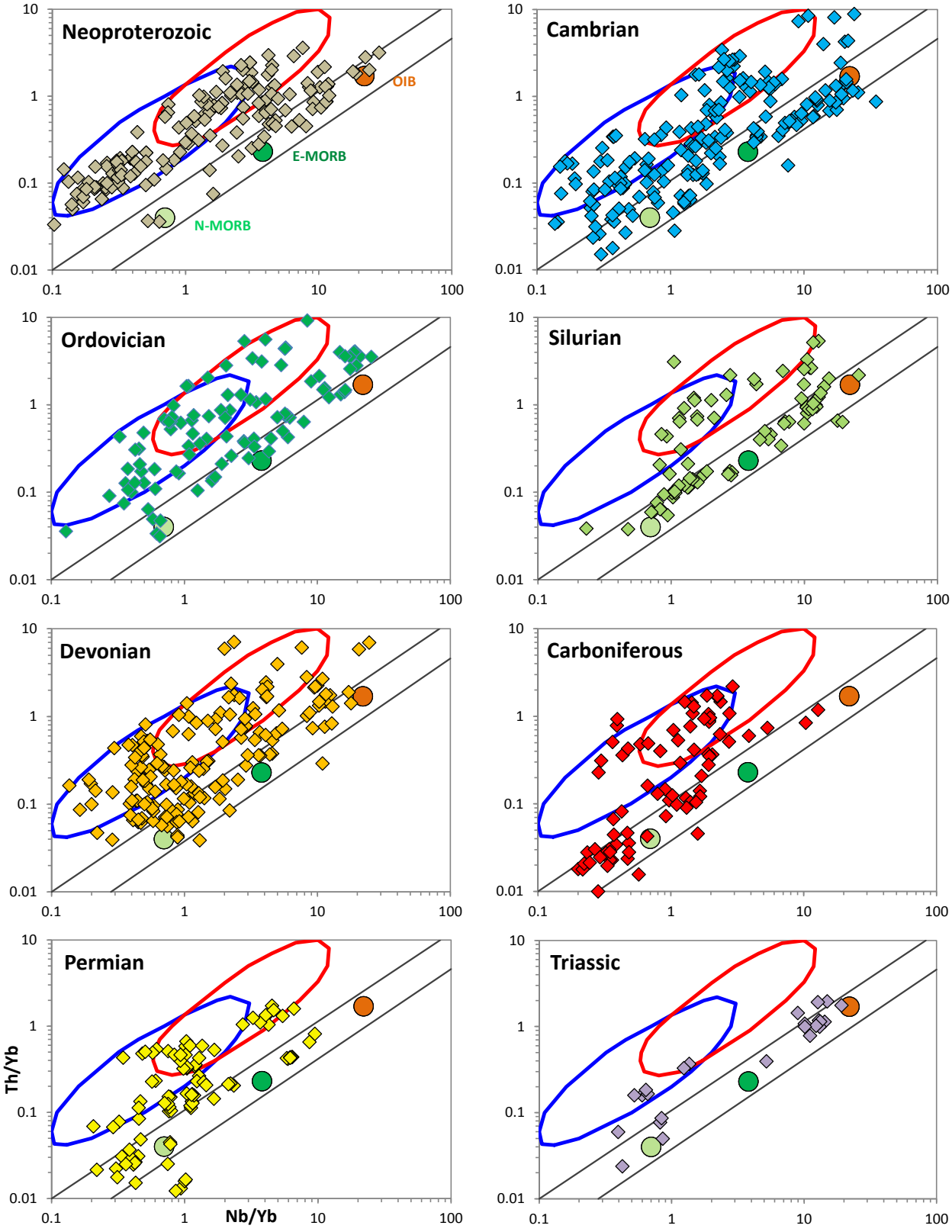


**Figure 10.** Th/Yb–Nb/Yb plots of the metabasalts of the Neoproterozoic through Triassic ophiolite complexes.

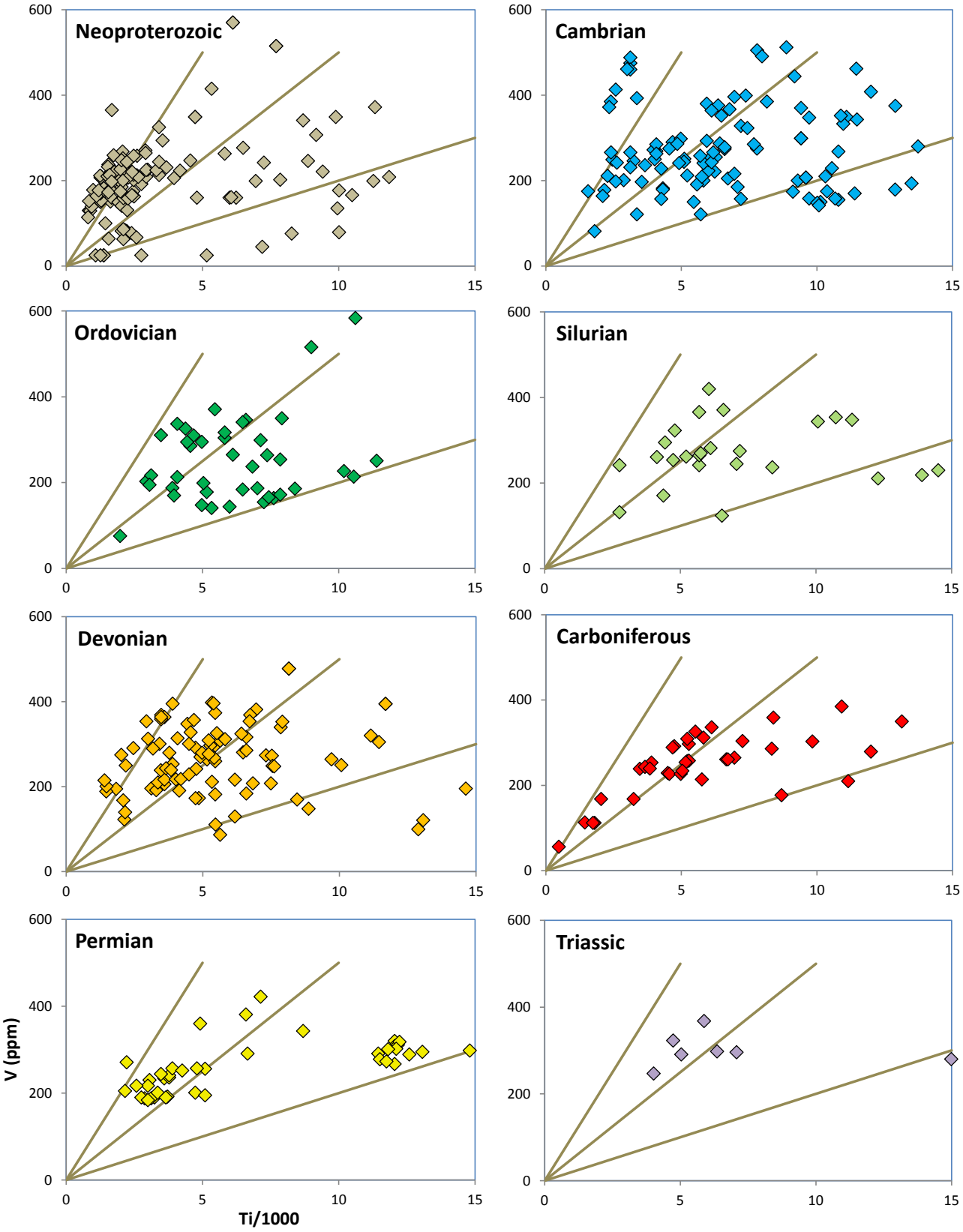


**Figure 11.** V–Ti/1000 plots of the metabasalts of the Neoproterozoic through Triassic ophiolite complexes.

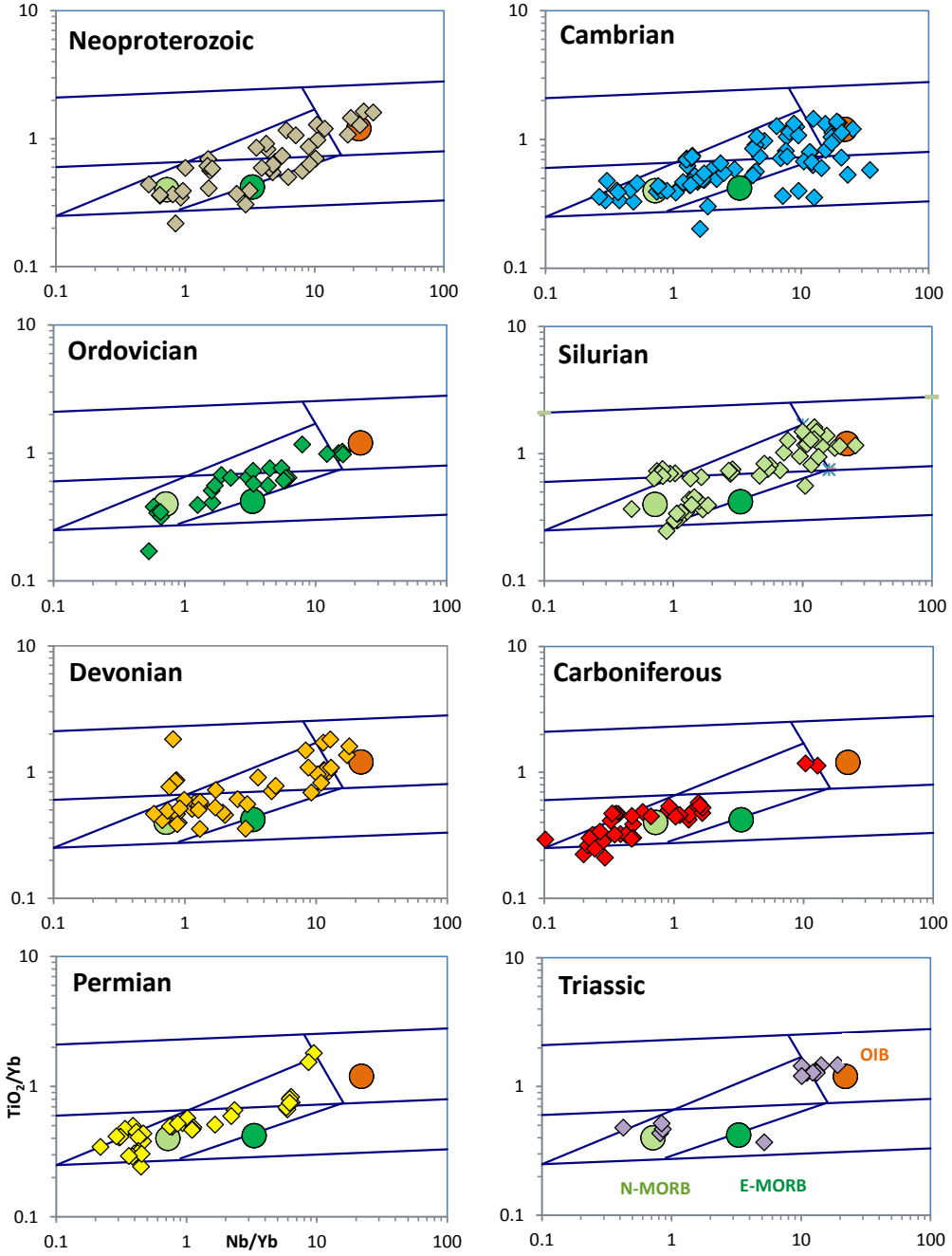


**Figure 12.** $TiO_2$–Nb/Yb plots of the metabasalts of the Neoproterozoic through Triassic ophiolite complexes.

Two of the complexes (Iradyr and Bingdaban) show flat to depleted multi-element pattern, and with low element concentrations, i.e., ca. 4–20 times PM (Fig. 8B). The basalts of the Ordovician complexes mostly define Th-enriched patterns and negative Nb-anomalies, except those from the Wudashimen complex which define a flat, depleted (similar to N-MORB) pattern (Fig. 8C). Some do also show minor to marked negative Zr-anomalies (Imanburluk and Tulinkai complexes), negative Sm-anomalies (Aermantai complex), and pronounced negative P-anomalies for the Huoshishan-Niujianzi complex (Fig. 8C). The patterns of the PM-normalized basalts of the Silurian complexes are flat (Serikeyayilake complex) to moderately incompatible-element-enriched, and only a minor part shows negative Nb-anomalies (Fig. 8D). The basalts of all of the Devonian complexes show slight to strong enrichment with increasing incompatibility of the elements, and most of them define moderate to strong (mainly) negative Nb-anomalies (Fig. 8E). The basalts from about half of the Carboniferous complexes define flat patterns and slight to moderate enrichment (towards the most incompatible elements), and with minor to major negative Nb-anomalies in the PM-normalized multi-element diagrams (Fig. 8F). The other half defines flat to slightly depleted character (the Eastern Erenhot) in the MORB-normalized multi-element diagrams (Fig. 8F). Some of the basalts of the Permian complexes define flat pattern (e.g., Daqing Pasture), but the majority define slight to significant enriched (e.g., Kuznetsk Basin) multi-element patterns, and weak to significant negative

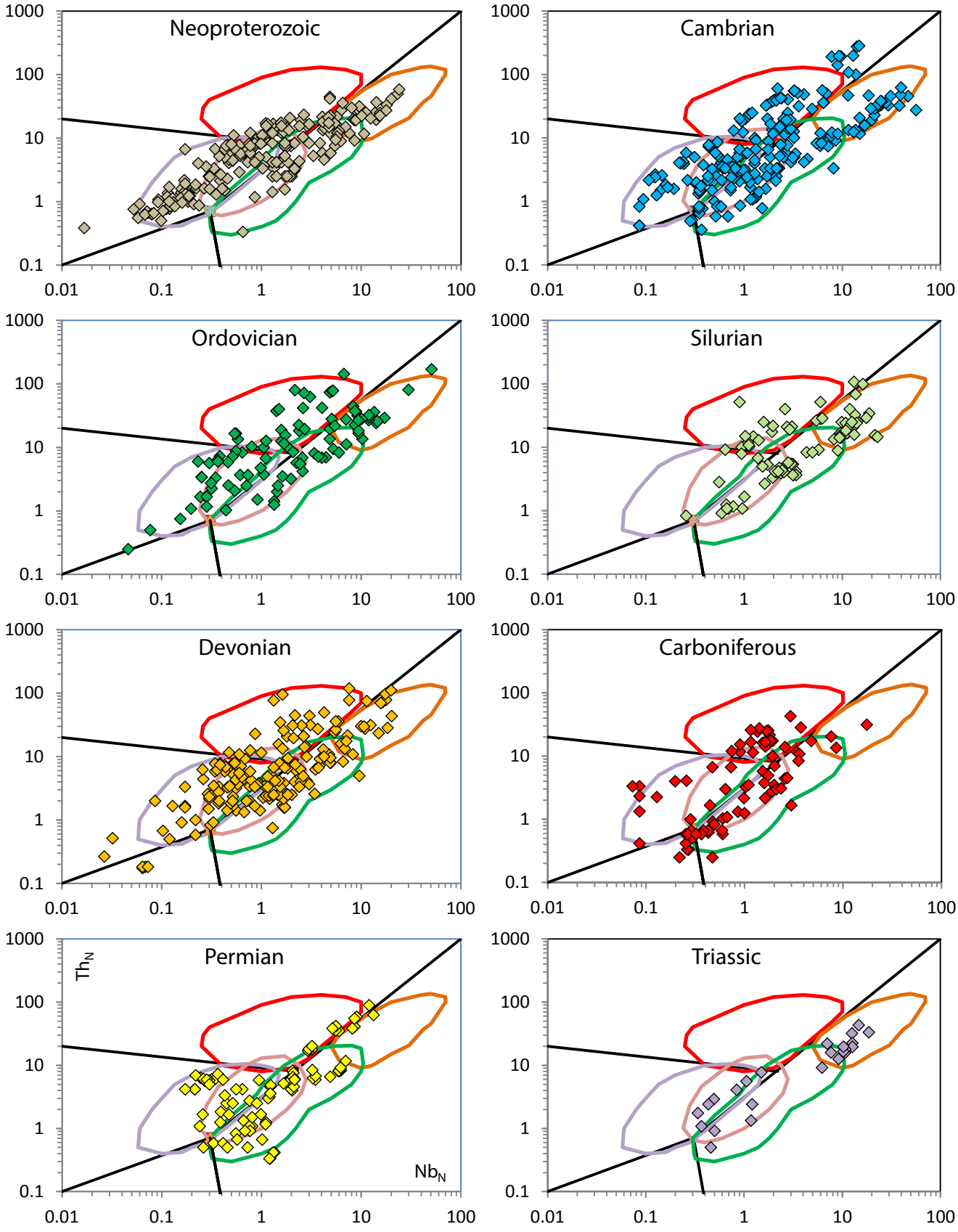


**Figure 13.** $Th_N$–$Nb_N$ plots of the metabasalts of the Neoproterozoic through Triassic ophiolite complexes.

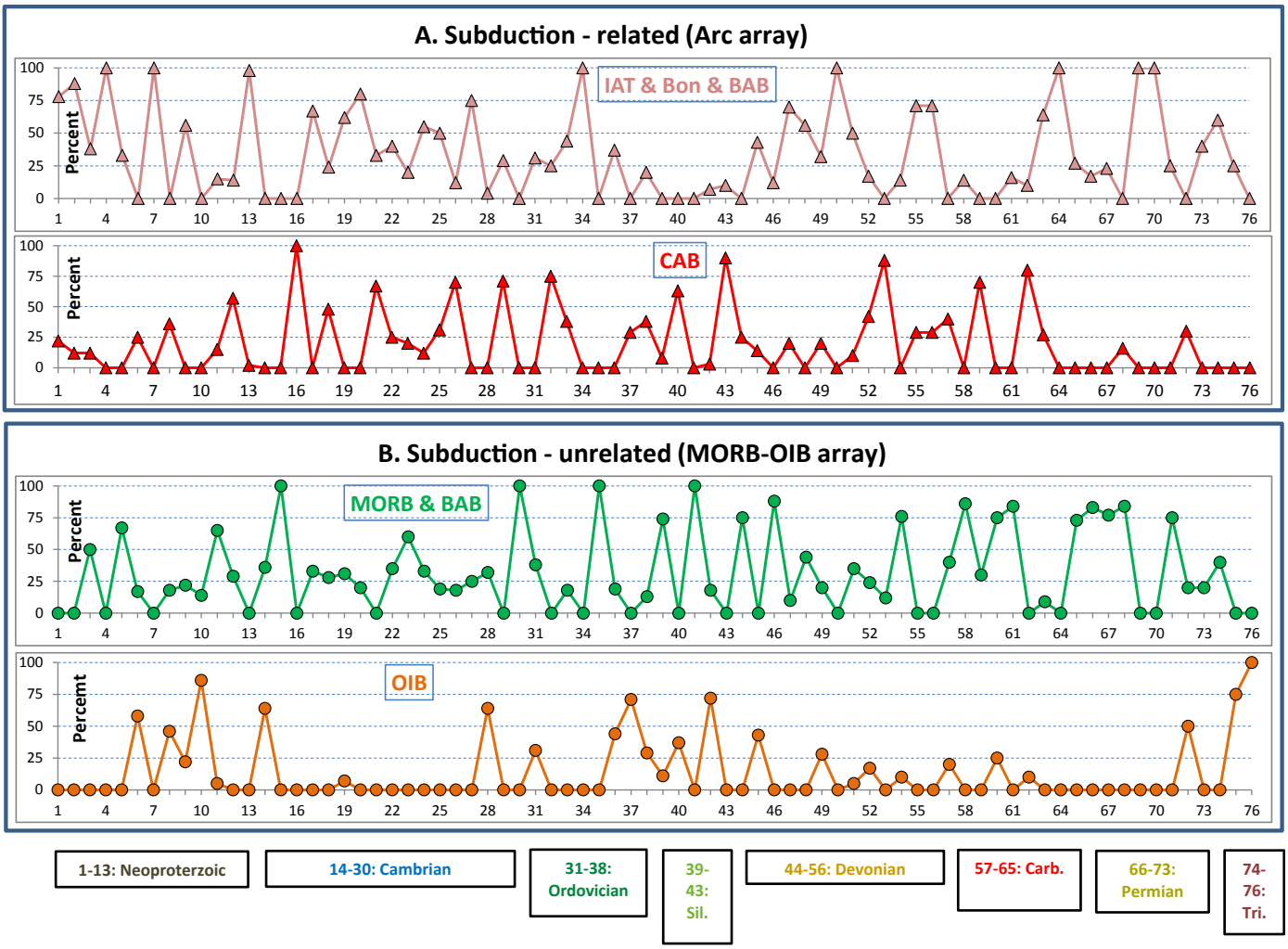


**Figure 14.** Subduction-related and subduction-unrelated character of each of the complexes of Neoproterozoic through Triassic ages. Numbers refer to the numbered complexes shown in Table 1 and Supplementary Table 2.

Nb-anomalies (Fig. 8G). The basalts of the Hegenshan complex define two types, i.e., one type without Nb-anomalies, and the other type showing depleted character with positive Nb-anomalies (Fig. 8G). The Triassic complexes, including only three complexes, show highly different PM-normalized multi-element patterns. While the basalts of the Aluchin complex define flat pattern with marked negative Nb-anomalies, the basalts of the Raohe and Heilongjiang define Th-enriched patterns, mainly without negative Nb-anomalies (Fig. 8H).

### 5.3. Discrimination diagrams

The elements Ti, Y, Zr, Nb, V, Th and Yb, applied either as various ratios or element concentration, have been plotted in the discrimination diagrams of Pearce (2014) and Saccani (2015), and the results are shown in Figs. 9–14.

The subduction influence (0–100%) in each of the complexes, as expressed in the discrimination diagrams of Pearce (2014) has been estimated. All samples that plot above the mantle array, i.e., in the Th/Yb –Nb/Yb diagram of Fig. 3 (step 2), and in the field of the volcanic arc array of Fig. 4, have been taken as influenced by subduction processes. The results are shown as histograms in Fig. 9A. In this calculation it is clear that the complexes that are insignificantly or entirely unaffected (0–10%) by subduction-related processes comprise a relatively small part, whereas those substantially to entirely subduction-influenced (90%–100%) comprise the major part. Further, all samples that show subduction-influence (in the Th/Yb–Nb/Yb diagram of Fig. 3, step 2) have been plotted in the V–Ti diagram of Fig. 3 (step 3), indicating fields of boninite, IAT, MORB and alkali basalts. The results of this compilation are shown in four histograms (for boninite, IAT, MORB and alkali basalt) in Fig. 9B1–B4. For the majority of the complexes boninite and alkali basalts are scarce or absent, whereas IAT and MORB occur in various proportion in all of the complexes (Fig. 9B2–B3). The samples that plot in the mantle array have further been plotted in the Nb/Yb–$TiO_2$/Yb diagram of Fig. 3 (step 4). This diagram separates the basalts that have originated from shallow melting (MORB array) from those of a deep melting environment (OIB array). The results are illustrated by two histograms in Fig. 9C1–C2, showing that the dominant part of the complexes have basalts of the MORB array.

The proportions (in terms of calculated percentages) of each of the occupied fields represented by the various time periods (Neoproterozoic through Triassic) are shown in Table 3. The calculated values for each of the seventy-three complexes are shown in Supplementary Tables 1 and 2. Fig. 10 shows the Th/Yb–Nb/Yb relationships for the Neoproterozoic through the Triassic complexes. The majority of the data exhibit subduction-influence, in particular, the Neoproterozoic and Ordovician complexes, while

**Table 3**
Summary of discrimination character (Pearce, 2014; Saccani, 2015) of the basaltic rocks of the CAOB.

| Discrimination (Pearce 2014) | Neoproterozoic | Cambrian | Ordovician | Silurian | Devonian | Carbonifeous | Permian | Triassic |
|---|---|---|---|---|---|---|---|---|
| **Nb/Yb - Th/Yb poxy (in %)** | | | | | | | | |
| Mantle | 17 | 36 | 21 | 58 | 25 | 40 | 36 | 58 |
| Weak subduction influence | 11 | 21 | 24 | 18 | 27 | 22 | 18 | 17 |
| Oceanic arc (OA) | 41 | 15 | 18 | 1 | 29 | 10 | 18 | 17 |
| Continental arc (CA) | 12 | 17 | 15 | 7 | 9 | 2 | 9 | 0 |
| Joint OC-CA | 19 | 11 | 22 | 16 | 10 | 26 | 19 | 8 |
| **Ti/V proxy( in %)** | | | | | | | | |
| Bon | 30 | 10 | 0 | 0 | 15 | 0 | 2 | 0 |
| IAT | 48 | 30 | 37 | 36 | 51 | 61 | 53 | 44 |
| MORB | 19 | 50 | 60 | 48 | 28 | 39 | 36 | 23 |
| Alk. Basalt | 3 | 10 | 3 | 16 | 6 | 0 | 9 | 33 |
| **Nb/Yb - $TiO_2$/Yb proxy (in %)** | | | | | | | | |
| N-MORB } MORB | 15 | 18 | 19 | 4 | 21 | 63 | 57 | 29 |
| E-MORB } array | 49 | 39 | 46 | 30 | 35 | 31 | 22 | 7 |
| OIB-tholeiite } OIB | 24 | 27 | 23 | 49 | 33 | 3 | 21 | 21 |
| OIB-alkaline } array | 12 | 16 | 12 | 21 | 11 | 3 | 0 | 43 |
| **Discrimination (Saccani 2015)** | | | | | | | | |
| **Subduction-related (in %)** | | | | | | | | |
| IAT & Bon & BAB | 47 | 30 | 30 | 6 | 40 | 20 | 29 | 29 |
| CAB | 15 | 23 | 24 | 18 | 16 | 26 | 9 | 0 |
| Sum | 62 | 53 | 54 | 24 | 56 | 46 | 38 | 29 |
| **Subduction-unrelated (in %)** | | | | | | | | |
| MORB & BAB | 28 | 36 | 28 | 53 | 35 | 53 | 58 | 30 |
| OIB | 10 | 11 | 18 | 23 | 9 | 1 | 4 | 41 |
| Sum | 38 | 47 | 46 | 76 | 44 | 54 | 62 | 71 |

those of Silurian age plot mainly within the MORB-OIB mantle array. For most of the complexes (of any age, except the Cambrian), the smallest contribution is represented by the continental arc composition (Table 3). Further, isolating the subduction-influenced samples in the V–Ti diagram (Fig. 11), the highest proportion of boninite and IAT appears in the Neoproterozoic and Devonian complexes (78% and 66%, respectively), whereas the highest proportion of MORB and alkali basalts (around 60%) occur in the Cambrian, Ordovician and Silurian complexes. Isolating the data of the OIB-MORB array (Fig. 3, step 4) in the Nb/Yb–$TiO_2$/Yb diagram (Fig. 12), the majority of the complexes define MORB character, i.e., derivation from shallow melting, while the Silurian and Triassic complexes show a predominance of OIB character, indicating deep melting.

The MORB-normalized Nb and Th values of the Neoproterozoic through Triassic complexes have been plotted in a simplified version of the Saccani (2015) discrimination diagram (Fig. 13), and the estimated proportions of subduction-related and subduction-unrelated data shown in Table 3. The highest proportion of subduction-related basalts are in the Neoproterozoic, Cambrian, Ordovician and Devonian complexes, with values (in %) of 62, 53, 54 and 56, respectively, and the proportion of calc-alkaline basalts (CAB) is relatively minor to moderate. For the Silurian, Carboniferous, Permian and Triassic complexes the subduction-related proportions are all less than 50% (Table 3). The subduction-unrelated varieties are dominated by MORB type basalts (except for the Triassic).

In order to best possibly visualize the time-related geochemical development of the complexes one by one, we present the percentages of the arc array (IAT/Bon/BAB and CAB) and the MORB-OIB array (MORB/BAB and OIB) for the Neoproterozoic through Triassic periods in Fig. 14. This illustration (Fig. 14) is based on the simplified version (see Fig. 4) of the discrimination diagram of Saccani (2015), and shows the calculated proportions of arc array fields IAT/Bon/BAB and CAB, and the MORB-OIB array fields MORB/BAB and OIB, for each individual complex. The complexes have been numbered (1–76), and the numbers correspond to those shown in Table 1 and Supplementary Table 2. For the subduction-related arc array, about 25% of the complexes do not plot in the joint IAT/Bon/BAB field, whereas the remaining 75% of the complexes define minor to major contribution. As to the CAB field, geochemical data from 50% of the complexes plot within this field, of which the highest concentrations are present in the Cambrian, Silurian and Carboniferous complexes, whereas the Permian and Triassic complexes define sparse contribution.

For the subduction-unrelated MORB-OIB array, about 30% of the complexes do not plot in the MORB/BAB field, whereas the remaining 70% of the complexes define a sparse to major (100%) contribution in this field. Particularly the data from the Carboniferous and Permian complexes are significantly represented. For the

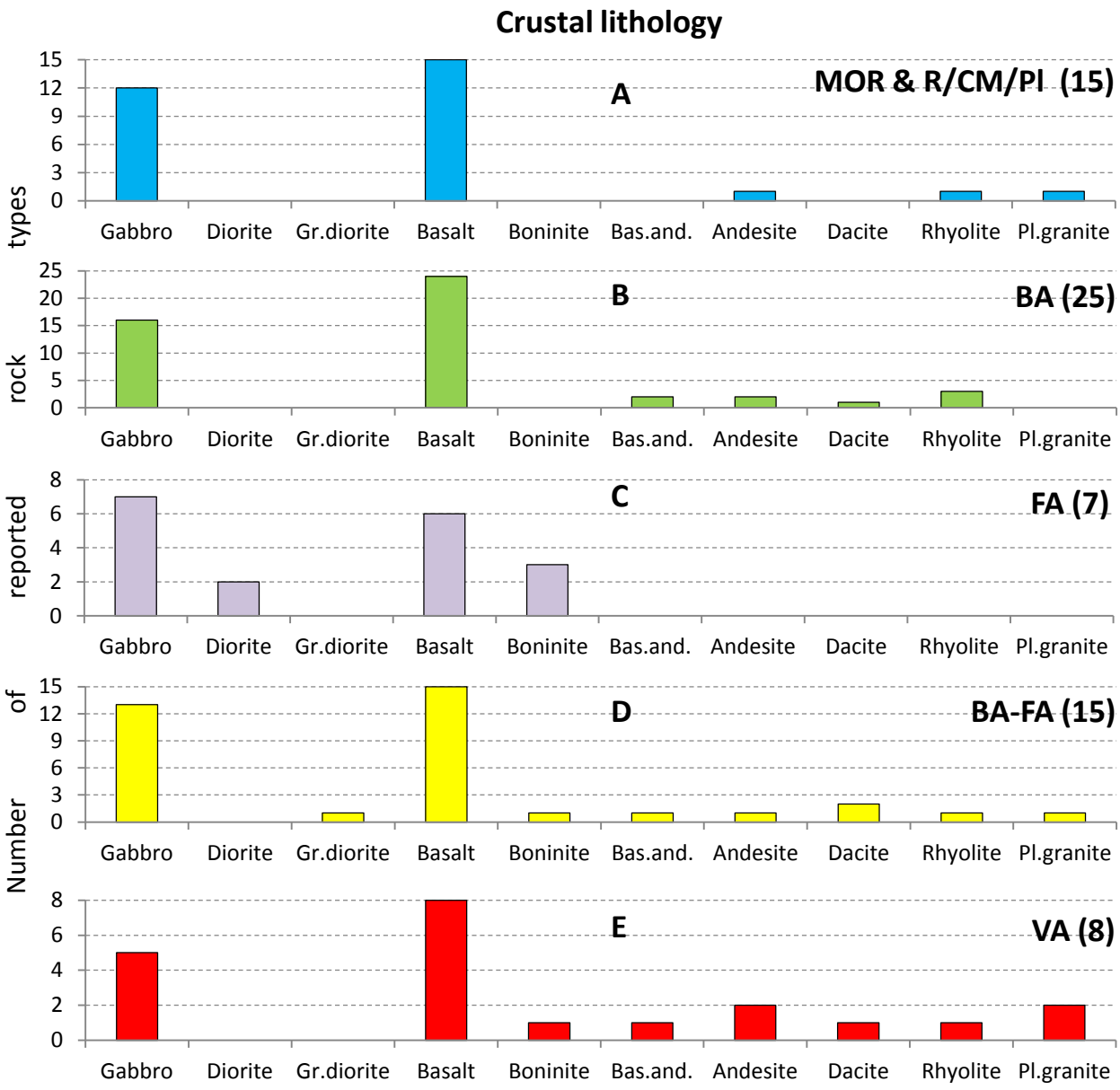


**Figure 15.** Relationship between crustal rock types of the investigated complexes and their geochemical composition. The number in parenthesis (after each ophiolite type) denotes the number of complexes.

Cambrian, Devonian, Carboniferous and Permian complexes, the OIB contribution is sparse, whereas for those of Neoproterozoic, Ordovician and Triassic ages, OIB contribution is significant (Fig. 14).

## 6. Lithology versus geochemistry

### 6.1. Crustal rocks

Fig. 15 illustrates relationships between the reported crustal lithological components of the different complexes as listed in Table 1, and the proposed ophiolite type primarily based on the geochemical characteristic as shown in Figs. 10 and 11. A common feature for all the complexes is the general occurrence of gabbro and basalt. As pointed out above, the backarc type oceanic crust may structurally look like MOR–generated oceanic lithosphere, and in terms of rock types represented, they are rather similar, as also shown in Fig. 15A and B. Oceanic crust generated in forearc region (producing FA type ophiolite) of a subduction-related environment may share structural and lithological similarities with that of the MOR oceanic crust (particularly in its lower sections) by the invariable appearance of gabbro and basalt, but differs from the subduction-unrelated and the BA type ophiolites by the presence of abundant boninitic extrusive and intrusive rocks (Fig. 15C). Similarly, the Backarc to Forearc (BA–FA) ophiolites, considered as a hybrid type between that of BA and FA ophiolites, also exhibit a wider variety of rock components than those of BA type (Fig. 15D). Whereas subduction-unrelated ophiolites, as well as those of the subduction-related BA, BA-FA and FA types are entirely dominated by basaltic extrusive and gabbroic intrusive rocks, those of the longer-lived VA type (Dilek et al., 1991; Dilek and Furnes, 2011, 2014) are characterized by a dominance of diorite, tonalite and granodiorite intrusions in the middle to lower crust (see Fig. 1 of Furnes and Dilek, 2017), and show a wide variety of extrusive rocks

**Table 4**
Suggested ophiolite types and associated complexes of the CAOB.

| Complex/area | Reference(s) to geochemical data and previously suggested tectonic setting | Suggested ophiolite type based on discrimination diagrams of Pearce (2014) and Saccani (2015) | Associated complex |
|---|---|---|---|
| **Neoproterozoic** | | | |
| Eastern Sayan oph. | | | |
| Dunzhugur (Dr) & | Forearc, arc, backarc; Sklyarov et al. (2016) | Forearc | |
| Ilchir (Il) | Forearc; Belyaev et al. (2017) | Forearc | |
| | Kuzmichev and Larionov (2013) | | |
| Shishkid (Sd) | Backarc; Kuzmichev et al. (2005) | Backarc to Forearc | OIB |
| Katun 1 (Kt1) | Mid-ocean ridge; Safonova et al. (2011) | Backarc | MORB |
| Kurai (Kr) | Mid-oc. ridge + Oc. isl. magmatism; Safonova et al. (2008) | Backarc | OIB, OPB |
| Bayankhongor (BH) | Suprasubduction; Buchan (2001) | MOR | Volcanic arc, OIB |
| | Mid-ocean ridge; Jian et al. (2010) | | |
| Jifeng (Jg) | Suprasubduction type; Feng et al. (2016) | *Forearc* | |
| Gorif (Gf) | Subduction-accretion & oc.crust/seamount | Backarc | OIB |
| | Volkova and Budanov (1999) | | |
| Shatskii (Sk) | Oc. Isl. & prim. isl.arc: Mongush et al. (2011) | Backarc + plume | |
| Mayile (Me) | Intra-oceanic setting; Wang et al. (2003); Yang et al. (2012c) | Rift/Plume | OIB |
| Agardagh | Backarc basin/isl.arc; Pfänder et al. (2002) | Backarc to Forearc | OIB |
| Tes-Chem (ATC) | | | |
| Khantaishir 1 (Kh1) | Incipient arc; Gianola et al. (2014); Janousek et al. (2018) | *Forearc* | |
| Khantaishir 2 (Kh2) | Forearc; Gianola et al. (2017) | Forearc | |
| **Cambrian** | | | |
| Katun 2 (Kt2) | Plume; Safonova et al. (2011a); Safonova and Santosh, (2014) | MOR | Plume/OIB |
| Dzhalair-Naiman (DN) | Ophiolite; Degtyarev (2012) | *MOR* | |
| Biluutiin ovoo (Bo) | Suprasubduction; Zhu et al. (2014) | Volcanic Arc | |
| Yueyashan-Xichangjian (YX) | Backarc; Ao et al. (2012) | Backarc to Forearc | OIB? |
| Hongliuhe (He) | Suprasubduction; Cleven et al. (2015) | Volcanic Arc | |
| Chagantaolegai (Cg) | Mid-ocean ridge; Zhao and He (2014) | Backarc | OIB? |
| Katun 3 (Kt3) | Suprasubduction; Safonova et al. (2011) | Backarc | |
| Zoolen (Zl) | Forearc; Jian et al. (2014) | *Forearc* | |
| Kherlen (Kn) | Suprasubduction; Miao et al. (2016) | Forearc | |
| S. Hövsgöl Hl) | Isl.arc or oc.isl. Medvedev et al. (2008) | Backarc to Forearc | |
| Boshchekul (Bl) | Ophiolite; Degtyarev (2012) | Backarc to Forearc | |
| Chistopol (Cl) | Mid-ocean ridge; Degtyarev et al. (2016) | MOR/Rift | |
| Iradyr (Ir) | Mid-ocean ridge; Degtyarev et al. (2016) | *Backarc* | |
| Zasur'ya (Zs) | Mid-ocean ridge and oceanic islands; Safonova et al. (2011) | MOR/Plume | OIB |
| Selety-Urumbai | Intra-oceanic arc; Degtyarev (2012); Safonova et al. (2017) | *Volcanic Arc* | |
| (Shiil Fm.) (SU) | | | |
| Bingdaban (Bb) | Mid-ocean ridge; Dong et al. (2007) | MOR | |
| **Ordovician** | | | |
| Itmurundy (Iy) | Mid-ocean ridge, forearc; Safonova et al. (2018c) | Backarc | OIB, MORB |
| Imanburluk (Ik) | Backarc basin; Degtyarev et al. (2016) | *Backarc* | |
| Aermantai (Ai) | Oceanic crust; Wang et al. (2003) | Volcanic Arc | |
| Tulinkai (Tk) | Suprasubduction zone; Jian et al. (2008) | *Backarc to Forearc* | |
| Wudaoshimen (Wn) | Backarc extension; Song et al. (2015) | *MOR* | |
| Kurtushiba (Ka) | Oc. Plateau & isi.arc; Volkova et al. (2009) | Backarc | OIB |
| Huoshishan-Niujuanzi (HN) | Suprasubduction setting; Tian et al. (2014) | *Backarc* | *OIB* |
| Zhaheba (Zb) | Suprasubduction; Luo et al. (2017) | Backarc to Forearc | OIB |
| **Silurian** | | | |
| Alegedayi (Ay) | Intra-arc spreading; Wong et al. (2010) | Backarc | OIB |
| Aertengkesi (Ak) | Suprasubducton type; Jiang et al. (2014) | Backarc | |
| Serikeyayilake (Se) | Suprasubduction type; Jiang et al. (2014) | MOR | |
| S. Tianshan (ST) | Mid-ocean ridge to Iceland-type plume; Safonova et al. (2016) | MOR/Backarc (?) | Plume/OIB |
| Edrengiin Nuru (EN) | Ensimatic/-sialic island arc; Badarch et al. (2002) | Volcanic Arc | |
| **Devonian** | | | |
| Tseel (Tl) | Juvenile backarc; Demouz et al. (2009) | *Backarc* | |
| Heiyingshan (Hn) | Backarc basin; Wang et al. (2011) | Backarc | |
| Dalabute (De) | Mid-ocean ridge; Liu et al. (2014b) | Backarc | |
| Darbut (Db) | Backarc basin; Yang et al. (2012b) | Backarc to Forearc | |
| Baijiantan- | Mid-ocean ridge; Zhu et al. (2015) | Backarc | |
| Baikouquan (BB) | | | |
| Sartuohai (Si) | Plume activity; Yang et al. (2012a) | Volcanic Arc | OIB |
| Karamaili (Kl) | Oceanic crust; Wang et al. (2003) | Backarc to Forearc | |
| Xinjiang (Xg) | MORB/backarc/withing plate; Liu et al. (2011) | Backarc to Forearc | |
| E. Junggar 1 (EJ1) | Immature to mature arc; Zhang et al. (2009) | Backarc to Forearc | OIB |
| Nyrnin-Sagan Gp (NS) | Suprasubduction/rift; Kruk et al. (2008) | Volcanic Arc | |
| Char (Ch1) | Oceanic; Safonova et al. (2012) | Backarc | OIB, MORB |
| Char (Ch2) | Intra-oceanic arc; Kurganskaya et al. (2014) | *Backarc to Forearc* | |
| Char (Ch3) | intra-oceanic arc; Safonova et al. (2018a,b) | Backarc to Forearc | |
| **Carboniferous** | | | |
| E. Junggar 2 (EJ2) | Backarc/volcanic arc; Zhang et al. (2009) | *Backarc* | |
| Xi-Ujimqi (XU) | Backarc extension; Song et al. (2015) | MOR | |
| Xiaohuangshan (Xn) | Arc-basin system; Zheng et al. (2013) | Volcanic Arc | |

(*continued on next page*)

**Table 4** (*continued*)

| Complex/area | Reference(s) to geochemical data and previously suggested tectonic setting | Suggested ophiolite type based on discrimination diagrams of Pearce (2014) and Saccani (2015) | Associated complex |
|---|---|---|---|
| Guluogou (Gn) | Mid-ocean ridge type; Jiang et al. (2014) | MOR | OIB |
| Khuhu Davaa (KD) | Initial stage of subd.; Zhu et al. (2017) | Backarc | |
| Shaquanzi (Sq) | Intracont. Backarc basin; Jiang et al. (2017) | Backarc | |
| Yuejinshan (Ye) | Mid-ocean ridge; Zhou et al. (2014); Wang et al. (2016) | Backarc to Forearc | |
| Diyanmiao (Do) | Backarc extension; Song et al. (2015) | Backarc | |
| Eastern Erenhot (Eh) | Backarc environment; Zhang et al. (2015) | MOR | |
| **Permian** | | | |
| Daqing Pasture (DP) | Backarc extension; Song et al. (2015) | *Backarc/(MOR ?)* | |
| Hegenshan (Hs) | Suprasubduction zone; Miao et al. (2008) | Backarc | OIB |
| Liuyuan (La) | Forearc; Mao et al. (2012) | Backarc | |
| Dongfanghong (Dg) | Immature arc; Sun et al. (2015) | Forearc | |
| Solonker (Sk) | Continental margin type; Luo et al. (2016) | *Backarc to Forearc* | OIB |
| Heilongjiang North (H1) | Rift setting; Zhou et al. (2009) | *Rift* | *OIB* |
| Kuznetsk Basin (KB) | Plume/SSZ source; Nastavko et al. (2012) | Plume/Volcanic Arc | traps |
| Manlay (My) | Suprasubduction; Zhu et al. (2014) | Backarc to Forearc | |
| **Triassic** | | | |
| Aluchin (An) | Suprasubduction basin; Ganelin (2011) | Backarc | |
| Heilongjiang South (H2) | Rift to subduction; Zhou et al. (2009) | *Backarc* | *OIB* |
| Raohe (Re) | Ocean island; Zhou et al. (2014) | Plume | OIB |

In Kursiv: < 8 samples; 13 complexes of 75 (i.e. 17%).

from basalt, andesite, dacite and rhyolite (Fig. 15E). Even though many of the complexes most probably do not contain all original lithologies, Fig. 14 shows that the geochemical classification (Table 4) reflects the lithological construction of the complexes.

### 6.2. Mantle rocks

The mantle rocks are invariably dominated by harzburgite and dunite, and wehrlite is also common in some cases (Fig. 16A–E). All the ophiolites carry peridotite and serpentinite suggesting various mantle rocks. Lherzolite is rather uncommon, and has not been reported in the FA type ophiolites (Fig. 16C). In the forearc region, with the common appearance of boninites, generated from highly depleted mantle, its absence accords with the geochemical classification.

### 6.3. Metamorphic grade

The metamorphic grade of the reported ophiolites varies from low grade through blueschist. The term *low grade* includes variants such as "weakly metamorphosed, sub-greenschist, low–T alteration and hydrothermal alteration" (Table 1). Most of the ophiolites are characterized by having undergone low grade and greenschist metamorphism (Fig. 17A–E). Only the subduction-unrelated and BA type ophiolites exhibit amphibolite to blueschist metamorphic grades (Fig. 17A and B; Table 1). Subduction-related ophiolites most probably represent the upper plate of subduction systems, whereas subduction-unrelated ophiolites may instead represent the downgoing plate and thus get subjected to high-P metamorphic grade (blueschist grade). Blueschist metamorphic conditions have been reported from several of the investigated complexes from the oldest to the youngest, but eclogites, on the other hand, have not been reported from these complexes (see Table 1). There are, however, numerous occurrences of eclogite connected to several suture zones within the CAOB (e.g., Ota et al., 2002; Javkhlan et al., 2013; Xiao et al., 2014; Pilitsyna et al., 2018).

## 7. Discussion

As shown in Supplementary Tables 1 and 2 the geochemical proxies for the different ophiolite types differ significantly, and one ophiolite type may grade into another type. Thus, in some cases it may be difficult to classify the ophiolite to one specific type. Different ophiolite types with 0 to 100% subduction contribution may occur adjacent to each other, as for example demonstrated by the Katun ophiolites (units 2 and 3) of Russian Altai or by the Char ophiolites of East Kazakhstan (Safonova et al., 2011a, 2012, 2018a; Supplementary Tables 1 and 2).

When treating the geochemical data as outlined in Figs. 3 and 4, we classified the selected ophiolitic sequences of the CAOB according to the various tectonic settings as outlined in Fig. 2; the compilation is shown in Fig. 18, and summarized in Table 4. Further, Fig. 19 illustrates the ophiolite classification represented in a pie-diagram, outlining the ophiolites types classified as Backarc (BA), Backarc to Forearc (BA–FA), Forearc (FA), and Volcanic arc (VA), constitute 35%, 22%, 16% and 10%, respectively, making the subduction-related ophiolites a dominant group (79%). Of the remaining 21% the MOR type makes up the major part (16%) and the R/CM/P type the last 5% (Fig. 19). Below is a brief discussion of the environment in which the subduction-unrelated group of ophiolites may be generated, and the processes that may lead to the diversity of the subduction-related group of ophiolites.

### 7.1. Subduction-unrelated ophiolites

For the subduction-unrelated category, i.e. showing geochemical affinities to OIB (enriched in LREE, Nb, Ti and with differentiated HREE) and different from subduction-related magmas in the absence of negative Nb anomalies, the question that arises is whether these ophiolites formed at rifted continental margins, at an initial stage that further developed to become back-arc spreading centers, or were triggered by mantle plumes within oceanic plates (of any age). Fig. 2A shows that either scenario are possible, and an appropriate example of subduction-unrelated segments of otherwise subduction-influenced backarc crust, though of apparently minor volumetric significance, is provided by the active Scotia Sea backarc (Fretzdorff et al., 2002). Seamounts and ocean islands that may have a plume origin are common in all the major modern and fossil oceans (e.g., Hofmann, 1997; Regelous et al., 2003; Staudigel and Clague, 2010; Safonova and Santosh, 2014). They may also occur in backarc basins (e.g., see Fig. 22.1 of

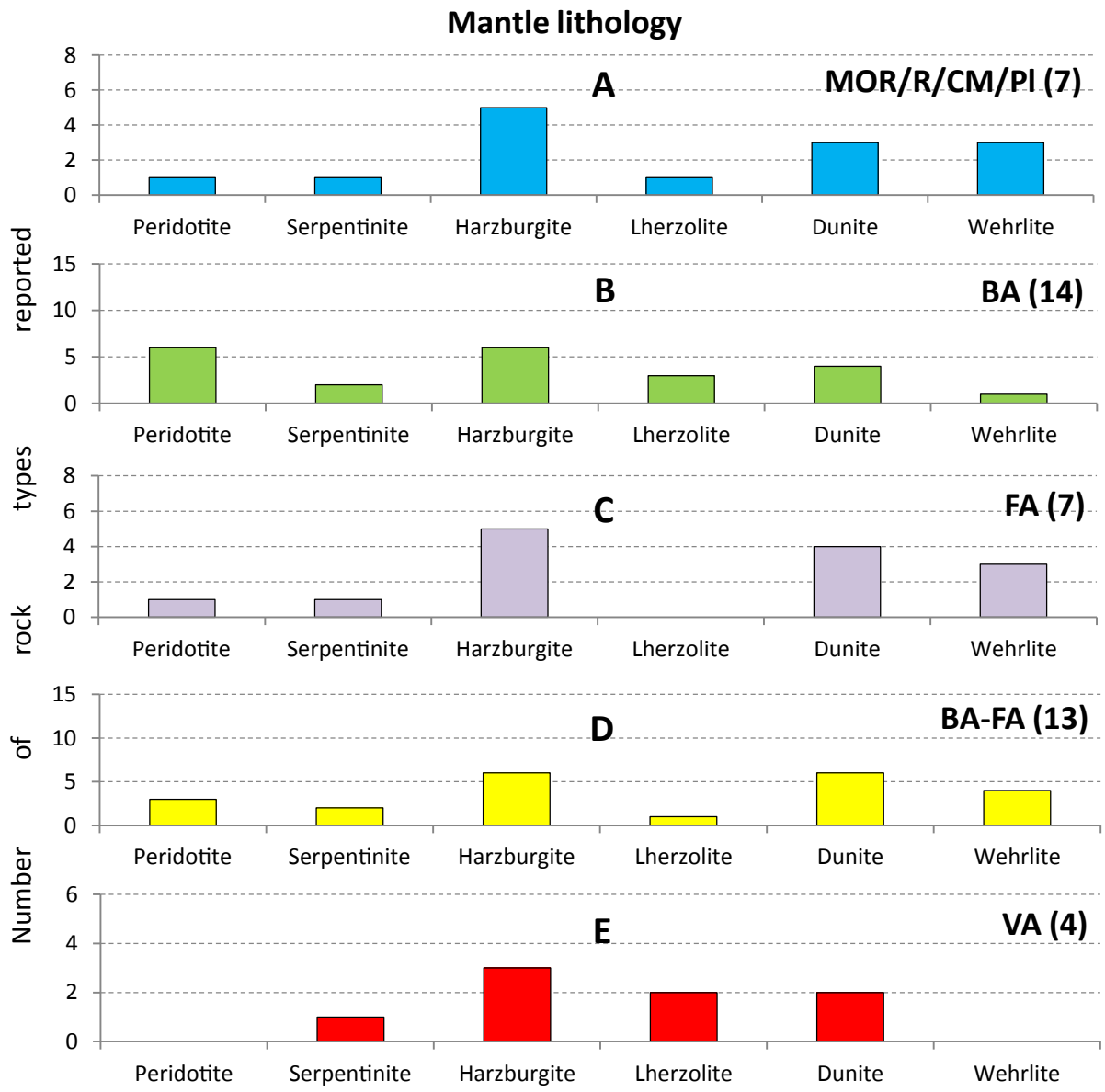


**Figure 16.** Relationship between mantle rock types of the investigated complexes and their geochemical composition. The number in parenthesis (after each ophiolite type) denotes the number of complexes.

Staudigel and Koppers, 2015). Both oceanic island/seamount and backarc basalts compositionally define very wide geochemical ranges (Leat et al., 2000; Fretzdorff et al., 2002; Keller et al., 2002; Regelous et al., 2003; Tararin et al., 2003; Pearce et al., 2005; Safonova et al., 2011; Yan et al., 2012; Jafri and Sheikh, 2013; Beier et al., 2015). For example, calc-alkaline basalts occur at seamounts of the Andaman Sea (Kamesh Raju et al., 2012; Tripathi et al., 2017), and Mariana Trough (Fryer et al., 1997). More examples can be found in the Nascent backarc basin behind the Shichito Ridge, NW Pacific (Ikeda and Yuosa, 1989), on the Oki-Dogo and Jejudo islands in the backarc region of the Sea of Japan (Nakamura et al., 1989; Tatsumi et al., 2005), in the Lau Basin (Gill, 1976), the Daito Basin in the Philippine Sea (Marsh et al., 1980; Hickey-Vargas, 1998), and the Bransfield Strait, Antarctica (Fisk, 1990). Also, seamounts of both calc-alkaline character (Marsili seamount; Trua et al., 2002) and alkaline character (Vavilov Seamount; Robin et al., 1987) occur in the Tyrrhenian backarc basin. Thus, some seamounts registered in backarc basins represent magmatic development related to the subducting slab, whereas others may relate to backarc spreading centers and/or plume activity. Further, seamounts of tholeiitic to alkaline character occurring on the seafloor of backarc basins, and which have the geochemical characters consistent with plume activity, might represent traces of former plumes that originally were responsible for the opening of the backarc basins (e.g., Hickey-Vargas, 1998; Macpherson and Hall, 2001; Deschamps and Lallemand, 2002; Sdrolias et al., 2004; Barnes, 2008; Deschamps et al., 2008; Ishizuka et al., 2013; Chang et al., 2016). Thus, the presence of seamounts in backarc basins, even though of alkaline character, may be indicative of active plume development.

Based on the geochemical interpretation of all the selected ophiolitic complexes, about 40% are associated with alkaline ocean island basalts (OIBs). For those classified as subduction-unrelated, 60% are associated with OIB (Table 4). This compares well with the identification of plume-related alkaline basalts associated with OPS within many of the accretionary complexes of the CAOB and

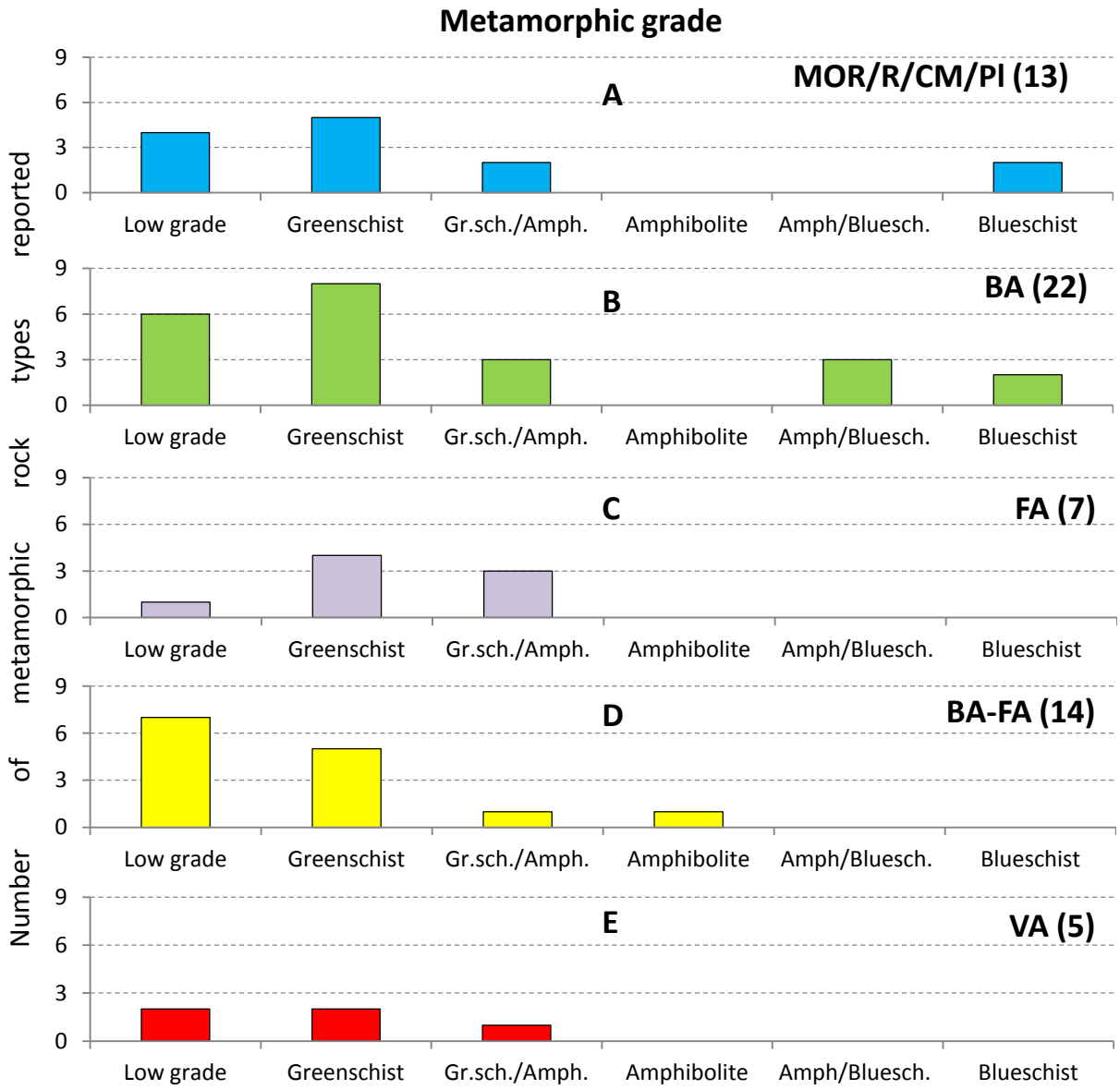


**Figure 17.** Relationship between metamorphic rock types of the investigated complexes and their geochemical composition. The number in parenthesis (after each ophiolite type) denotes the number of complexes.

the Western Pacific (Safonova and Santosh, 2014 and references cited therein). These relationships would suggest formation of the subduction-unrelated ophiolites at intra-plate oceanic rises (seamounts, islands) in major oceans rather than formation within a backarc basin. Subduction-unrelated ophiolites that represent oceanic crust that belongs to the downgoing plate may suffer high-pressure, subduction-zone metamorphism. The metamorphic grade of the present examples that have been classified as subduction-unrelated ophiolites varies from low greenschist to blueschist (Table 1) or even to eclogite, thus showing that the various complexes were subducted to different depths before exhumation.

### 7.2. Subduction-related ophiolites

A combination of several processes may account for the large geochemical variations of subduction-produced signatures over short distances. One explanation for the differences in subduction contribution along a subduction zone is the variation in the dip-angle. In the active subduction systems around the Pacific Ocean, the dip-angle of subduction show large variation from $<30°$ to near-vertical (e.g., Gvirtzman and Stern, 2004; Lallemand et al., 2005), and the slab geometry may vary laterally as well as time-wise at a fixed position (Guillaume et al., 2013). It is particularly in basins with backarc spreading that the steepest dips occur ($>51°$), whereas in the case of backarc shortening the dips $< 31°$ (Lallemand et al., 2005). Further, as demonstrated by Lallemand et al. (2005) the slab-dip is controlled by the upper plate strain, the absolute motion of the overriding plate, as well as the absolute motion of the arc/trench. Thus, lateral variations in the dip-angle of the subducting slab within a backarc basin may account for the extent of subduction influence of the mantle at the spreading centres, which again accounts for the different classification of the ophiolite complexes. Also, the change of spreading centres within backarc basins may be related to ridge jumps. This is a process that is well documented at both mid-ocean ridges in major oceans (e.g.,

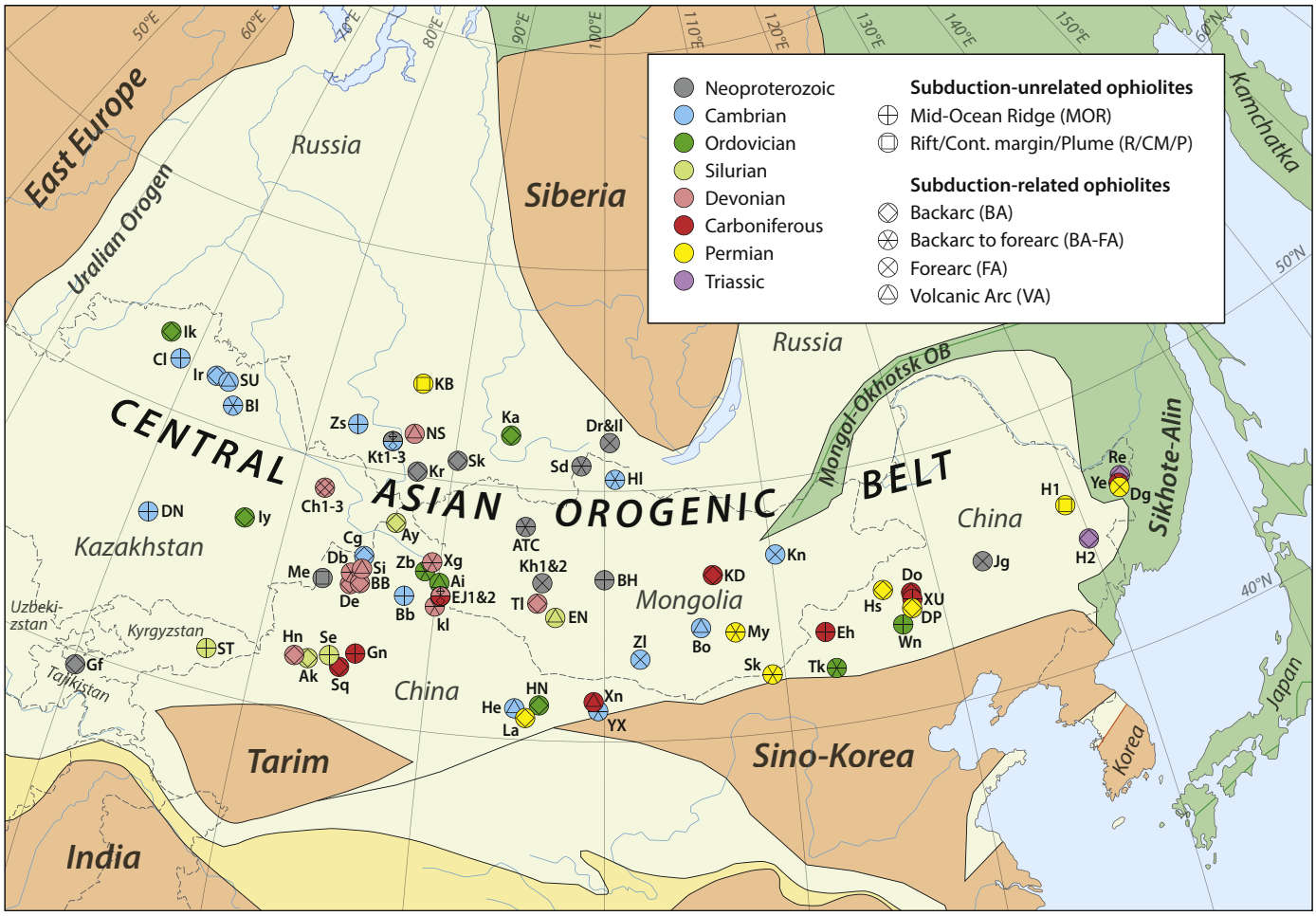


**Figure 18.** Outline of the Central Asian Orogenic Belt (modified from Safonova and Santosh, 2014), showing the geographical position of the Neoproterozoic to Triassic investigated complexes, and the classification into different ophiolite types.

Mittelstaedt et al., 2008), and in backarc basins. For the backarc basins, the West Philippine Basin (Deschamps et al., 2008), the Scotia Sea (Maldonado et al., 2014), and the Gulf of Mexico (Stern and Dickinson, 2010) can be mentioned as examples.

Another element that may contribute to the lateral difference in the subduction contribution is the subduction rate. The global subduction rates during Cenozoic time show considerable variation from ca. 1.5 to 16 cm/year (Hoareau et al., 2015), and in the same subduction system the rates may vary by ca. 2 cm/year within short time intervals of 1–2 Ma (Hoareau et al., 2015). The amount of sediments that is dragged down within a subduction zone (e.g., von Huene and Scholl, 1991; Clift and Vannucchi, 2004; Scholl and Van Huene, 2007; Safonova et al., 2015) and which may carry high concentration of important subduction-related elements (e.g., Th, see Plank and Langmuir, 1998) may vary significantly, and thus contribute to the geochemical differences as demonstrated by the suprasubduction ophiolites as represented by the four (BA, BA-FA, FA, and VA) subduction-related types.

### 7.3. *Proportions of subduction-related and subduction-unrelated ophiolites in the CAOB*

As show in Fig. 19 the proportions of the subduction-related and subduction-unrelated ophiolites, which have been preserved in the CAOB, are 79% and 21%, respectively. The geological and geochronological data show at least 21 intra-oceanic arcs in the CAOB, not considering continental arcs (Safonova, 2017; Safonova et al., 2017). Moreover, a lot of intra-oceanic arc or continental arc material can be destroyed to form turbidite and graywacke sandstones deposited in trenches and fore-arc basins, respectively, and then subducted to the deep mantle (Yamamoto et al., 2009; Safonova et al., 2015). Recently, it has been shown that many fossil arcs of the Paleo-Asian Ocean, which closure formed the CAOB, disappeared from the surface leaving only their derived sandstones

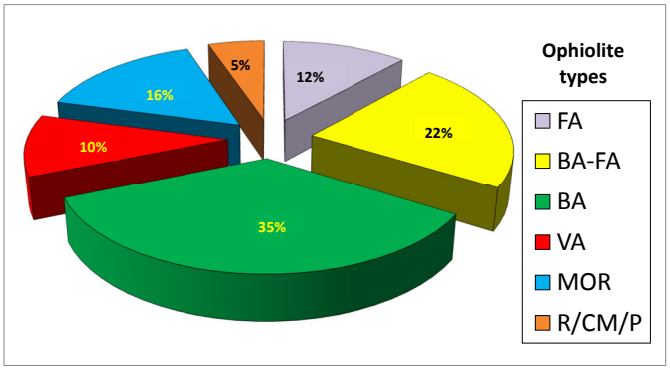


**Figure 19.** Pie diagram showing the proportion (in %) of each ophiolite type.

with unimodal distribution of U–Pb zircon ages and positive epsilon Hf characteristics (Safonova, 2017; Safonova et al., 2018b,c). Thus, the current proportions of subduction-related and subduction-unrelated ophiolites do not necessarily reflect their initial proportions and therefore must be interpreted with caution (Kröner et al., 2014, 2017). However, the proportion of subducted-related and subducted-unrelated ophiolites as shown in the compilation of this study is very similar to that of earlier studies. Thus, the subduction-related proportion of 118 Proterozoic ophiolites from several orogenic belts (Caledonian-Appalachian, Hercynian, Uralian, Maghebrian-Alpine-Himalayan, Caribbean, Central Asian-Qingling/Qilian/Kunlun, Gondwanide-Tasmanian, Western Pacific-Cordilleran, Indonesia-Myanmar) makes up 75% (Furnes et al., 2014). Further, a similar study of 105 greenstone sequences worldwide (North America/Canada, Greenland, Baltica (NW Russia, Finland and Norway), Siberia, China and Mongolia, SE Europe, South America, Africa, Arabian/Nubian Shield, India, Australia) shows that the estimated subduction-related ophiolites constitute 85% (Furnes et al., 2015). Although we must take into account the MOR ophiolites seldom remain on the surface but mostly get subducted to the deep mantle, it anyway appears that subduction-related ophiolites are by far the dominant ophiolitic unit remained on the surface of the Earth through all times, even in the early stages of the Earth. This supports the idea that Plate Tectonics and related subduction operated back to the early Archean (e.g., Furnes et al., 2007; Komiya et al., 2015; de Wit et al., 2018), or even in the Hadean (Maruyama et al., 2018).

## 8. Summary

Geochemical characterization of 73 ophiolitic complexes within the Central Asian Orogenic Belt, ranging in age from Neoproterozoic to Triassic, define a variety of subduction-unrelated and subduction-related types, and show the following features:

(1) The ophiolites of subduction-related origin comprise the major group (about 79%), and can further be subdivided as Backarc (BA), Forearc (FA), Backarc to Forearc (BA–FA) and Volcanic Arc (VA) types.
(2) The BA type is by far the dominant type, followed by BA–FA, while FA and VA types are subordinate.
(3) The level of subduction influence is highly variable among the BA type ophiolites (varying of 10%–100%), while it is invariably high (90%–100%) in the FA type. The BA-FA and VA types define intermediate levels of subduction influence between the two end member types (BA and FA).
(4) The Neoproterozoic and Ordovician complexes exhibit the highest, whereas those of Silurian age exhibit the lowest subduction-influence.
(5) The MOR type ophiolites are the dominant group amongst the subduction-unrelated group, but their relations to adjacent subduction-related ophiolites, indicate that a significant amount also formed in backarc basins, but without subduction influence.
(6) Harzburgite, dunite, gabbro and basalt are common lithologies in all ophiolite types, whereas the BA-FA, FA and VA types generally contain intermediate to felsic rocks, and in the FA type boninites occur.
(7) The subduction-related ophiolites types generally show low metamorphic grade, whereas greenschist, amphibolite and blueschist grades occur in the subduction-unrelated and BA types.
(8) About 40% of all the selected ophiolitic complexes are associated with alkaline ocean island basalts (OIBs), and for those classified as subduction-unrelated, 60% are associated with OIB, as oceanic islands/seamount/plateaus survive better during subduction.
(9) The substantial difference in the subduction influence (from 0 to 100%) between adjacent ophiolites may attest to variable dips of the subducting slab laterally, as well as the variable amounts of hydrated sediments and subduction-important elements (as f.ex. Th) transported down the subduction zone and variable flux of into the mantle, which affect the composition of the melts generated over the subducting slab.
(10) Subduction-related ophiolites as a dominant ophiolitic unit remained on the Earth through all times thus supporting the idea that Plate Tectonics and related subduction operated back to the early Archean.

## Acknowledgements

Vasilly Belyaev is thanked for help in getting information and geochemical data from the Eastern Sayan ophiolites. Tuo Jiang and Jun Gao are thanked for helping to get papers from various Chinese journals containing geochemical data from ophiolite complexes. We are grateful to an anonymous reviewer who pointed out several issues in an early version of the manuscript that have been taken care of and hence resulted in an improvement of the final text. We thank Eva Bjørseth for helping with some of the illustrations. Harald Furnes was supported by the Department of Earth Science, University of Bergen, Norway. Inna Safonova was supported by the Ministry of Education and Science of the Russian Federation, grant # 14.Y26.31.0018, Russian Foundation for Basic Research (Grant # 16-05-00313) and Scientific Project of IGM SB RAS No. 0330-2016-0003. This paper is a contribution to IGCP#662.

## Appendix A. Supplementary data

Supplementary data to this article can be found online at https://doi.org/10.1016/j.gsf.2018.12.007.

## References

Anonymous, 1972. Penrose field conference on ophiolites. Geotimes 17, 24–25.
Ao, S.J., Xiao, W.J., Han, C.M., Li, X.H., Qu, J.F., Zhang, J.E., Guo, Q.Q., Tian, Z.H., 2012. Cambrian to early Silurian ophiolite and accretionary processes in the Beishan collage, NW China: implications for the architecture of the Southern Altaids. Geological Magazine 149 (4), 606–625.
Badarch, G., Cunningham, W.D., Windley, B.F., 2002. A new terrane subdivision for Mongolia: implications for the Phanerozoic crustal crustal growth of Central Asia. Journal of Asian Earth Sciences 21, 87–110.
Barnes, G.L., 2008. The making of the Japan Sea and the Japanese Mountains: understanding Japan's volcanism in structural context. Japan Review 20, 3–52.
Beier, C., Bach, W., Turner, S., Niedermeier, D., Woodhead, J., Erzinger, J., Krumm, S., 2015. Origin of silicic magmas at spreading centres –an example from the south east rift, manus basin. Journal of Petrology 56 (2), 255–272.
Belyaev, V.A., Wang, K.L., Gornova, M.A., Dril, S.-I., Karimov, A.A., Medvedev, A.Y., Noskova, Yu, V., 2017. Geochemistry and origin of the eastern sayan ophiolites, Tuva-Mongolian microcontinent (southern Siberia). Geodynamics & Tectonophysics 8 (3), 411–415. https://doi.org/10.5800/GT-2017-8-3-0250.
Biske, Y.S., Seltmann, R., 2010. Paleozoic tian-Shan as a transitional region between the rheic and urals-turkestan oceans. Gondwana Research 17, 602–613.
Buchan, A.C., 2001. Tectonic Evolution of the Bayankhongor Ophiolite, Central Mongolia: Implications for the Palaeozoic Crustal Growth of Central Asia. PhD thesis. University of Leicester, p. 179.
Buslov, M.M., Safonova, I.Yu, Watanabe, T., Obut, O., Fujiwara, Y., Iwata, K., Semakov, N.N., Sugai, Y., Smirnova, L.V., Kazansky, A.Yu, 2001. Evolution of the Paleo-Asian Ocean (Altai-Sayan region, Central Asia) and collision of possible Gondwana-derived terranes with the southern marginal part of the Siberian continent. Geosciences Journal 5, 203–224.
Chang, S.-J., Ferreira, A.M.G., Faccenda, M., 2016. Upper and mid-mantle interaction between the Samoan plume and the Tonga-Kermadec slabs. Nature Communications 7. https://doi.org/10.1038/ncomms10799.
Cleven, N., Lin, S., Guilmette, C., Xiao, W., Davis, B., 2015. Petrogenesis and implications for tectonic setting of Cambrian suprasubduction-zone ophiolitic rocks in the central Beishan orogenic collage, Northwest China. Journal of Asian Earth Sciences 113, 369–390.

Clift, R., Vannucchi, P., 2004. Controls on tectonic accretion versus erosion and recycling of the continental crust. Reviews of Geophysics 42, RG2001. https://doi.org/10.1029/2003RG000127.
Degtyarev, K.E., 2012. Tectonic Evolution of the Early Paleozoic Island Arc Systems and Formation of the Continental Crust in the Caledonides of Kazakhstan. GEOS, Moscov, p. 2012.
Degtyarev, K.E., Tolmacheva, T.Yu, Tretyakov, A.A., Kotov, A.B., Shatagin, K.N., 2016. Cambrian to lower ordovician complexes of the kokchetav massif and its fringing (northern Kazakhstan): structure, age, and tectonic settings. Geotectonics 50 (1), 71–142.
Demoux, A., Kröner, A., Hegner, E., Badarch, G., 2009. Devonian arc-related magmatism in the Tseel terrane of SW Mongolia: chronological and geochemical evidence. Journal of the Geological Society, London 166, 459–471.
Deschamps, A., Lallemand, S., 2002. The West Philippine Basin: an Eocene to early-Oligocene backarc basin opened between two opposed subduction zones. Journal of Geophysical Research 107 (12). doi:10.102972001JB001706.
Deschamps, A., Shinjo, R., Matsumoto, T., Lee, C.-S., Lallemand, S.E., Wu, S., Scientific party of KR03 and KR04 cruises, 2008. Propagators and ridge jumps in a back-arc basin, the west Philippine Basin. Terra Nova 20, 327–332.
De Wit, M., Furnes, H., MacLennoan, S., Doucouré, M., Schoene, B., Weckmann, U., Martinez, U., Bowring, S., 2018. Paleoarchean bedrock lithologies across the Makhonjwa Mountains of South Africa and Swaziland linked to geochemical, magnetic and tectonic data reveal early plate tectonic genes flanking subduction margins. Geoscience Frontiers 9, 603–665.
Didenko, A.N., Mossakovskiy, A.A., Pecherskiy, D.M., Ruzhentsev, S.G., Samygin, S.G., Kheraskova, T.N., 1994. Geodynamics of paleozoic oceans of central Asia. Russian Geology and Geophysics 35, 48–62.
Dilek, Y., 2006. Collision tectonics of the Eastern Mediterranian region: causes and consequences. Geological Society of America Special Paper 409, 1–13.
Dilek, Y., Furnes, H., 2011. Ophiolite genesis and global tectonic fingerprinting of ancient oceanic lithosphere. The Geological Society of America Bulletin 123 (3/4), 387–411.
Dilek, Y., Furnes, H., 2014. Ophiolites and their origins. Elements 10, 93–100.
Dilek, Y., Thy, P., Moores, E.M., 1991. Episodic dike intrusion in the northwestern Sierra Nevada, California: implications for multistage evolution of a Jurassic arc terrane. Geology 19, 180–184.
Dilek, Y., Furnes, H., Shallo, M., 2008. Geochemistry of the Jurassic Mirdita ophiolite (Albania) and the MORB to SSZ evolution of a marginal basin oceanic crust. Lithos 100, 174–209.
Dilek, Y., Thy, P., 2009. Island arc tholeiite to boninitic melt evolution of the Cretaceous Kizildag (Turkey) ophiolite: model for multi-stage early arc – forearc magmatism in Tethyan subduction factories. Lithos 113 (1/2), 68–87.
Dobretsov, N.L., Buslov, M.M., Vernikovsky, V.A., 2003. Neoproterozoic to early ordovician evolution of the Paleo-Asian Ocean: implications to the break-up of rodinia. Gondwana Research 6, 143–159.
Dong, Y.P., Zhang, G.W., Zhou, D.W., Luo, J.H., Zhang, C.L., Xia, L.Q., Xu, X.Y., Ll, X.M., 2007. Geology and geochemistry of the Bingdaban ophiolitic mélange in the boundary fault zone on the northern Central Tianshan Belt, and its tectonic implications. Science in China - Series D: Earth Sciences 50 (1), 17–24.
Donskaya, T.V., Gladkochub, D.P., Mazukabzov, A.M., Ivanov, A.V., 2013. Late Paleozoic – mesozoic subduction-related magmatism at the southern margin of the Siberian continent and the 150 million-year history of the Mongol-Okhotsk Ocean. Journal of Asian Earth Sciences 62, 79–97.
Feng, Z., Liu, Y., Liu, B., Wen, Q., Li, W., Liu, Q., 2016. Timing and nature of the xinlin-xiguitu ocean: constraints from ophiolitic gabbros in the northern great xing'an range, eastern central asian orogenic belt. International Journal of Earth Sciences 105, 491–505.
Fisk, M.R., 1990. Volcanism in the Bransfield Strait, Antarctica. Journal of South American Earth Sciences 3 (2/3), 91–101.
Floyd, P.A., Winchester, J.A., 1975. Magma type and tectonic setting discrimination using immobile elements. Earth and Planetary Science Letters 27, 211–218.
Fretzdorff, S., Livermore, R.A., Devey, C.W., Leat, P.T., Stoffers, P., 2002. Petrogenesis of the back-arc East Scotia ridge, South Atlantic ocean. Journal of Petrology 43 (8), 1435–1467.
Fryer, P., Gill, J.B., Jackson, M.C., 1997. Volcanological and tectonic evolution of the Kasuga seamounts, northern Mariana Trough: alvin submersible investigations. Journal of Volcanology and Geothermal Research 79, 277–311.
Furnes, H., Dilek, Y., 2017. Geochemical characterization and petrogenesis of intermediate to silicic rocks in ophiolites: a global synthesis. Earth-Science Reviews 166, 1–37.
Furnes, H., de Wit, M., Staudigel, H., Rosing, M., Muehlenbachs, K., 2007. A vestige of Earth's oldest ophiolite. Science 315, 1704–1707.
Furnes, H., Robins, B., de Wit, M.J., 2012. Geochemistry and petrology of lavas in the upper onverwacht suite, Barberton mountain land, South Africa. South African Journal of Geology 115 (2), 171–210.
Furnes, H., de Wit, M., Dilek, Y., 2014. Four billion years of ophiolites reveal secular trends in oceanic crust formation. Geoscience Frontiers 5, 571–603.
Furnes, H., Dilek, Y., de Wit, M., 2015. Precambrian greenstone sequences represent different ophiolite types. Gondwana Research 27, 649–685.
Ganelin, A.V., 2011. Geochemistry and geodynamic significance of the dike series of the Aluchin Ophiolite Complex, Verkhoyansk-Chukotka fold zone, Northeast Russia. Geochemistry International 49 (7), 654–675.
Gao, J., Li, M.G., Xiao, X.C., Tang, Y.Q., He, G.Q., 1998. Palaeozoic tectonic evolution of the Tianshan Orogen, northwestern China. Tectonophysics 287, 213–231.
Gianola, O., Schmidt, M.W., Jagoutz, O., Sambuu, O., 2017. Incipient boninitic arc crust built on denudated mantle: the Khantaishir ophiolite (western Mongolia). Contributions to Mineralogy and Petrology 172, 92. https://doi.org/10.1007/s00410-017-1415-4.
Gill, J.B., 1976. Composition and age of Lau Basin and Ridge volcanic rocks.Implications for evolution of an interarc basin and remnant arc. The Geological Society of America Bulletin 87, 1384–1395.
Guillaume, B., Husson, L., Funiciello, F., Faccenna, C., 2013. The dynamics of laterally variable subductions: laboratory models applied to the Hellenides. Solid Earth 4, 179–200.
Gvirtzman, Z., Stern, R.J., 2004. Bathymetry of Mariana trench-arc system and formation of the Challenger Deep as a consequence of weak plate coupling. Tectonics 23, TC2011. https://doi.org/10.1029/2003TC001581.
Helo, C., Hegner, E., Kröner, A., Badarch, G., Tomuttogoo, O., Windley, B.F., Dulski, P., 2006. Geochemical signature of paleozoic accretionary complexes of the central asian orogenic belt in south Mongolia: constraints on arc environments and crustal growth. Chemical Geology 227, 236–257.
Hickey-Vargas, R., 1998. Origin of the Indian Ocean-type isotopic signature in the basalts from Philippine Sea plate spreading centers: an assessment of local versus large-scale processes. Journal of Geophysical Research 103 (B9), 20963–20979.
Hirschman, M.M., Stolper, E.M., 1996. A possible role for garnet pyroxenite in the origin of the "garnet signature" in MORB. Contributions to Mineralogy and Petrology 124, 185–208.
Hoareau, G., Bomou, B., van Hinsbergen, D.J.J., Carry, N., Marquer, D., Donnadieu, Y., Le Hir, G., Vrielynck, B., Walter-Simonnet, A.-V., 2015. Did high Neo-Tethyan subduction rates contribute to early Cenozoic warming? Climate of the Past 11, 1751–1767.
Hofmann, A.W., 1997. Mantle geochemistry: the message from oceanic volcanism. Nature 385, 219–229.
Hofmann, A., Wilson, A.H., 2007. Silicified basalts, bedded cherts and other sea floor alteration phenomena of the 3.4 Ga Nondweni greenstone belt, South Africa. In: Van Kranendonk, M.J., Smithies, R.H., Bennett, V.C. (Eds.), Earth's Oldest Rocks. Developments in Precambrian Geology 15. Elsevier, Amsterdam, pp. 571–605.
Ikeda, Y., Yuasa, M., 1989. Volcanism in nascent back-arc basins behind the Shichito Ridge and adjacent areas in the Izu-Ogasawara arc, northwest Pacific: evidence for mixing between E-type MORB and island arc magmas at the initiation of back-arc rifting. Contributions to Mineralogy and Petrology 101, 377–399.
Irvine, T.N., Baragar, W.R.A., 1971. A guide to the chemical classification of common volcanic rocks. Canadian Journal of Earth Sciences 8, 523–548.
Ishizuka, O., Taylor, R.N., Ohara, Y., Yuasa, M., 2013. Upwelling rifting and age-progressive magmatism from the Oki-Daito mantle plume. Geology 41 (9), 1011–1014. https://doi.org/10.1130/G34525.1.
Isozaki, Y., Maruyama, Sh, Fukuoka, F., 1990. Accreted oceanic materials in Japan. Tectonophysics 181, 179–205.
Jafri, S.H., Sheikh, J.M., 2013. Geochemistry of pillow basalts from bompoka, andaman-nicobar islands. Bay of bengal, Indian. Journal of Asian Earth Sciences 64, 27–37.
Jahn, B.-M., 2004. The central asian orogenic belt and growth of the continental crust in the phanerozoic. In: Malpas, J., Fletcher, C.J.N., Ali, J.R., Aitchison, J.C. (Eds.), Aspects of the Tectonic Evolution of China: Geological Society, London, Special Publication, vol. 226, pp. 73–100.
Janoušek, V., Jiang, Y., Buriánek, D., Schuimann, K., Hanžel, P., Soejono, I., Kröner, A., Altanbaatar, B., Erban, V., Lexa, O., Ganchuluun, T., Košler, J., 2018. Cambrian-ordovician magmatism of the ikh-mongol arc system exemplified by the khantaishir magmatic complex (lake zone, south-central Mongolia). Gondwana Research 54, 122–149.
Javkhlan, O., Takasu, A., Bat-Utzii, D., Kabir, Md F., 2013. Metamorphic pressure-temperature evolution of garnet-chloritoid schists from Lake Zone, SW Mongolia. Journal of Mineralogical and Petrological Sciences 108, 255–266.
Jian, P., Liu, D., Kröner, A., Windley, B.F., Shi, Y., Zhang, F., Shi, G., Miao, L., Zhang, W., Zhang, Q., Zhang, L., Ren, J., 2008. Time scale of an early to mid-Paleozoic orogenic cycle of the long-lived Central Asian Orogenic Belt, Inner Mongolia of China: implications for continental growth. Lithos 101, 233–259.
Jian, P., Kröner, A., Windley, B.F., Shi, Y., Zhang, F., Miao, L., Tomurhuu, D., Zhang, W., Liu, D., 2010. Zircon ages of the Bayankhongor ophiolite mélange and associated rocks: time constraints on Neoproterozoic to Cambrian accretionary and collisional orogenesis in central Mongolia. Precambrian Research 177, 162–180.
Jian, P., Kröner, A., Jahn, B-m., Windley, B.F., Shi, Y., Zhang, W., Zhang, F., Miao, L., Tomurhuu, D., Liu, D., 2014. Zircon dating of Neoproterozoic and Cambrian ophiolites in West Mongolia and implications for the timing of orogenic processes in the central part of the Central Asian Orogenic Belt. Earth-Science Reviews 133, 62–93.
Jiang, T., Gao, J., Klemd, R., Qian, Q., Zhang, X., Xiong, X., Wang, X., Tan, Z., Chen, B., 2014. Paleozoic ophiolitic mélanges from the South Tianshan Orogen, NW China: geological, geochemical and geochronological implications for the geodynamic setting. Tectonophysics 612–613, 106–127.
Jiang, H., Han, J., Chen, H., Zhen, Y., Lu, W., Deng, G., Tan, Z., 2017. Intra-continebtal back-arc basin inversion and late carboniferous magmatism in eastern tianshan, NW China: constraints from shaquanzi magmatic suite. Geoscience Frontiers 8, 1447–1467.
Kamesh Raju, K.A., Ray, D., Mudholkar, A., Murty, G.P.S., Gahalaut, V.K., Samudrala, K., Paropkari, A.L., Ramachandran, R., Surya Prakash, L., 2012. Journal of Asian Earth Sciences 56, 42–53.

Keller, R.A., Fisk, M.R., Smellie, J.L., Strelin, J.A., Lawver, L.A., 2002. Geochemistry of back arc basin volcanism in Bransfield Strait, Antarctica: subducted contributions and along-axis variations. Journal of Geophysical Research 107 (B8), 2171. https://doi.org/10.1029/2001JB000444.

Khain, E.V., Bibikova, E.V., Kröner, A., Zhuravlev, D.Z., Sklyarov, E.V., Fedotova, A.A., Kravchenko-Berezhnoy, I.R., 2002. The most ancient ophiolite of the Central Asian fold belt: U-Ph and Pb-Pb zircon ages for the Dunzhugur Complex, Eastern Sayan, Siberia, and geodynamic implications. Earth and Planetary Science Letters 199, 311–325.

Komiya, T., Maruyama, S., Hirata, T., Yurimoto, H., Nohda, S., 2004. Geochemistry of the oldest MORB and OIB in the Isua Supracrustal Belt, southern West Greenland: implications for the composition and temperature of early Archean upper mantle. Island Arc 13 (1), 47–72.

Komiya, T., Yamamoto, S., Aoki, S., Sawaki, Y., Ishikawa, A., Tashiro, T., Koshida, K., Shimojo, M., Aoki, K., Collerson, K.D., 2015. Geology of the Eoarchean, >3.95 Ga, Nulliak supracrustal rocks in the Saglek Block, northern Labrador, Canada: the oldest geological evidence for plate tectonics. Tectonophysics 662, 40–66.

Kovalenko, I., Aerov, G., Bagrova, Z., 1994. Geological and structural conditions localizing ornamental stone occurrences in the ophiolites of the Itmurunda Zone, Kazakhstan. In: Ishiwatari, et al. (Eds.), Proceeding of the 29th International Geological Congress Part D, pp. 255–262.

Kovalenko, V.I., Yarmolyuk, V.V., Kovach, V.P., Kotov, A.B., Kozakov, I.K., Salnikova, E.B., Larin, A.M., 2004. Isotope provinces, mechanisms of generation and sources of the continental crust in the Central Asian mobile belt: geological and isotopic evidence. Journal of Asian Earth Sciences 23, 605–627.

Kozakov, I.K., Kovach, V.P., Bibikova, E.V., Kirnozova, T.L., Zagornaya, N.Yu., Plotkina, Yu.V., Podkovyrov, V.N., 2007. Age and sources of granitoids in the junction zone of the Caledonides and Hercynides in southwestern Mongolia: Geodynamic implications. Petrology 15, 126–150.

Kröner, A., Rojas-Agramonte, Y., 2014. The Altaids as seen by eduard suess, and present thinking on the late mesoproterozoic to palaeozoic evolution of central Asia. Austrian Journal of Earth Sciences 107/1, 156–168.

Kröner, A., Kovach, V., Belousova, E., Hegner, E., Armstrong, R., Dolgopolova, A., Seltmann, R., Alexeiev, D.V., Hoffmann, J.E., Wong, J., Sun, M., Cai, K., Wang, T., Tong, Y., Wilde, S.A., Degtyarev, K.E., Rytsk, E., 2014. Reassessment of continental growth during the accretionary history of the central asian orogenic belt. Gondwana Research 25, 103–125.

Kröner, A., Kovach, V., Alexeiev, D.V., Wang, K.L., Wong, J., Degtyarev, K.E., Kozakov, I.K., 2017. No excessive crustal growth in the Central Asian Orogenic Belt: further evidence from field relationships and isotopic data. Gondwana Research 50, 135–166.

Kruk, N.N., Babin, G.A., Kruk, E.A., Rudnev, S.N., Kuibida, M.L., 2008. Petrology of volcanic and plutonic rocks from Uimen-Lebed' terrain, Gorny Altai. Petrology 16 (5), 512–530.

Kurganskaya, E.V., Safonova, I.Yu, Simonov, V.A., 2014. Geochemistry and petrogenesis of suprasubduction volcanic complexes of the Char shear zone, eastern Kazakhstan. Russian Geology and Geophysics 55, 69–84.

Kusky, T.M., Wang, L., Dilek, Y., Robinson, P., Peng, S., Huang, X., 2011. Application of modern ophiolite concept with special reference to Precambrian ophiolites. Science China Earth Sciences 54 (3), 315–341. https://doi.org/10.1007/s11430-011-4175-4.

Kusky, T., Windley, B., Safonova, I., Wakita, K., Wakabayashi, J., Polat, A., Santosh, M., 2013. Recognition of Ocean Plate Stratigraphy in accretionary orogens through Earth history: a record of 3.8 billion years of sea floor spreading, subduction, and accretion. Gondwana Research 24, 501–547.

Kuzmichev, A., Kröner, A., Hegner, E., Dunyi, L., Yusheng, W., 2005. The Shishkhid ophiolite, northern Mongolia: a key to the reconstruction of a Neoproterozoic island-arc system in central Asia. Precambrian Research 138, 125–150.

Kuzmichev, A.B., Larionov, A.N., 2013. Neoproterozoic island arcs in East Sayan: duration of magmatism (from U-Pb zircon dating of volcanic clastics). Russian Geology and Geophysics 54, 34–43.

Lallemand, S., Heuret, A., Boutelier, D., 2005. On the relationships between dip, back-arc stress, upper plate absolute motion, and crustal nature in subduction zones. Geochemistry, Geophysics, Geosystems 6 (9), Q09006. https://doi.org/10.1029/2005GC000917.

Leat, P.T., Livermore, R.A., Millar, I.L., Pearce, J.A., 2000. Magma supply in back-arc spreading centre segment E2, East Scotia Ridge. Journal of Petrology 41 (6), 845–866.

Le Maitre, R.W., 1989. A Classification of Igneous Rocks and Glossary of Terms. Blackwell, Oxford, UK.

Liu, X., Chen, B., Jahn, B-m., Wu, G., Liu, Y., 2011. Early paleozoic (ca. 465 Ma) eclogites from beishan (NW China) and their bearing on the tectonic evolution of the southern central asian orogenic belt. Journal of Asian Earth Sciences 42, 715–731.

Liu, X., Xu, J., Castillo, P.R., Xiao, W., Shi, Y., Feng, Z., Guo, L., 2014a. The the Dupal isotopic anomaly in the southern Paleo-Asian Ocean: Nd-Pb isotopic evidence from ophiolites in Northwest China. Lithos 189, 185–200.

Liu, X., Xiao, W., Xu, J., Castillo, P.R., Shi, Y., 2014b. Geochemical signature and rock associations of ocean ridge-subduction: evidence from the Karamaili Paleo-Asian ophiolite in east Junggar, NW China. Gondwana Research 48, 34–49.

Luo, Z-w., Xu, B., Shi, G-z., Zhao, P., Faure, M., Chen, Y., 2016. Solonker ophiolite in Inner Mongolia, China: a late Permian continental margin-type ophiolite. Lithos 261, 72–91.

Luo, J., Xiao, W., Wakabayashi, J., Han, C., Zhang, J., Wan, B., Ao, S., Zhang, Z., Tian, Z., Song, D., Chen, Y., 2017. The Zhaheba ophiolite complex in Eastern Junggar (NW China): long lived supra-subduction zone ocean crust and its implications for the tectonic evolution in southern Altaids. Gondwana Research 43, 17–40.

Lyubetskaya, T., Korenaga, J., 2007. Chemical composition of Earth's primitive mantle and its variance: 1. Method and results. Journal of Geophysical Research 112, B03211. https://doi.org/10.2029/2005JB004223.

Macpherson, C.G., Hall, R., 2001. Tectonic setting of Eocene boninite magmatism in the Izu-Bonin-Mariana forearc. Earth and Planetary Science Letters 186, 215–230.

Maldonado, A., Bohoyo, F., Galindo-Zaldívar, J., Hernández-Molina, F.J., Lobo, F.J., Lodolo, E., Martos, Y.M., Pérez, L.F., Schreider, A.A., Somoza, L., 2014. A model of oceanic development by ridge jumping: opening of the Scotia Sea. Global and Planetary Change 123, 152–173.

Mao, Q., Xiao, W., Windley, B.F., Han, C., Qu, J., Ao, S., Zhang, J., Guo, Q., 2012. The Liuyuan complex in the Beishan, NW China: a Carboniferous-Permian ophiolitic fore-arc sliver in the southern Altaids. Geological Magazine 149 (2), 483–506.

Marsh, N.G., Saunders, A.D., Tarney, J., Dick, H.J.B., 1980. Geochemistry of Basalts from the Shikoku and Daito Basins, Deep Sea Drilling Project Leg 58.Initial Reports Deep Sea Drilling Project 58, pp. 805–842.

Maruyama, S., Liou, J.G., Seno, T., 1989. Mesozoic and Cenozoic evolution of Asia: Oxford Monograph on Geology and Geophysics, pp. 75–99.

Maruyama, S., Liou, J.G., Terbayashi, M., 1996. Blueschist and eclogites of the world, and their exhumation. International Geology Review 38, 485–594.

Maruyama, S., Kawai, T., Windley, B.F., 2010. Ocean plate stratigraphy and its imbrication in an accretionary orogen: the Mona complex, Anglesey-Lleyn, 338. Geological Society, London, Special Publications, Wales, UK, pp. 55–75.

Maruyama, S., Santosh, M., Azuma, S., 2018. Initiation of Plate tectonics in the hadean: eclogitization triggered by ABEL bombardment. Geoscience Frontiers 9, 1033–1048.

Medvedev, A.Ya, Gordienko, I.V., Gornova, M.A., Almukhamedov, A.I., 2008. Geochemistry of metavolcanics in the southern Hövsgöl area (northern Mongolia): geodynamic implications. Russian Geology and Geophysics 49, 245–253.

Miao, L., Fan, W., Liu, D., Zhang, F., Shi, Y., Guo, F., 2008. Geochronology and geochemistry of the Heganshan ophiolitic complex: implixations for late-stage tectonic evolution of the Inner Mongolia-Daxinganling Orogenic Belt, China. Journal of Asian Earth Sciences 32, 348–370.

Miao, L., Baatar, M., Zhang, F., Anaad, C., Zhu, M., Yang, S., 2016. Cambrian Kherlen ophiolite in northeastern Mongolia and its tectonic implications: SHRIMP zircon dating and geochemical constraints. Lithos 261, 128–143.

Mittelstaedt, E., Ito, G., Behn, M.D., 2008. Mid-ocean ridge jumps associated with hotspot magmatism. Earth and Planetary Science Letters 266, 256–270.

Miyashiro, A., 1973. The Troodos ophiolitic complex was probably formed in an island arc. Earth and Planetary Science Letters 19, 218–224.

Mongush, A.A., Lebedev, V.I., Travin, A.V., corresponding Member of RAS V.V. Yarmolyuk, 2011. Ophiolites of western Tyva as fragments of a late Vendian island arc of the Paleo-Asian Ocean. Doklady Earth Sciences 438 (2), 866–872.

Moores, E.M., Vine, F.J., 1971. The Troodos massif, Cyprus, and other ophiolites as oceanic crust: evaluation and implications. Philosophical Transactions of the Royal Society London 268A, 443–466.

Nakamura, E., Campbell, I.H., McCulloch, M.T., Sun, S.-S., 1989. Geochemical geodynamics in a back arc region around the Sea of Japan: implications for the genesis of alkaline basalts in Japan, Korea, and China. Journal of Geophysical Research 94 (B4), 4634–4654.

Nastavko, A.V., Borodina, E.V., Izokh, A.E., 2012. Petrological and mineralogical features of volcanic rocks from the central Kuznetsk Basin (*southern Siberia*). Russian Geology and Geophysics 53, 334–346.

Ni, Z.Y., Zhai, M.G., Wang, R.M., Tong, Y., 2006. Late Paleozoic retrograded eclogites from within the northern margin of the North China Craton: evidence for subduction of the Paleo-Asian ocean. Gondwana Research 9, 209–224.

Niu, H., Sato, H.,H., Zhang, H., Ito, J., Yu, X., Nagao, T., Terada, K., Zhang, Q., 2006. Juxtaposition of adakite, boninite, high-$TiO_2$ and low-$TiO_2$ basalts in the Devonian southern Altay, Xinjiang, NW China. Journal of Asian Earth Sciences 28, 439–456.

Ota, T., Buslov, M.M., Watanabe, T., 2002. Metamorphic evolution of late precambrian eclogites and associated metabasites, gorny Altai, southern Russia. International Geology Review 44, 837–858.

Pa alakha, E.A., Belyi, V.A., 1981. Ophiolites of the itmurundy-kazyk zone. In: Abdulin, A.A., Patalakha, E.A. (Eds.), Ophiolites of Kazakhstan. Nauka, Alma-Ata, pp. 7–102.

Pearce, J.A., 2008. Geochemical fingerprinting of oceanic basalts with implications for the classification of ophiolites and search for Archean oceanic crust. Lithos 100, 14–48.

Pearce, J.A., 2014. Ophiolites: immobile elements fingerprinting of ophiolites. Elements 10 (2), 101–108.

Pearce, J.A., Cann, J.R., 1971. Ophiolite origin investigated by discriminant analysis using Ti, Zr and Y. Earth and Planetary Science Letters 12, 339–349.

Pearce, J.A., Cann, J.R., 1973. Tectonic setting of basic volcanic rocks determined using trace element analyses. Earth and Planetary Science Letters 19, 290–300.

Pearce, J.A., Norry, M.J., 1979. Petrogenetic implications of Ti, Zr, Y, and Nb variations in volcanic rocks. Contributions to Mineralogy and Petrology 69, 33–47.

Pearce, J.A., Parkinson, I.J., 1993. Trace element models for mantle melting: application to volcanic arc petrogenesis. In: Prichard, H.M., Alabaster, T.,

Harris, N.B.W., Neary, C.R. (Eds.), Magmatic Processes and Plate Tectonics: Geological Society of London, Special Publication, vol. 76, pp. 373–403.
Pearce, J.A., Lippard, S.J., Roberts, S., 1984. Characteristics and tectonic significance of supra-subduction zone ophiolites. Geological Society, London, Special Publications 16, 77–94.
Pearce, J.A., Stern, R.J., Bloomer, S.H., Fryer, P., 2005. Geochemical mapping of the Mariana arc-basin system: implications for the nature and distribution of subduction components. Geochemistry, Geophysics, Geosystems 6 (7), Q07006. https://doi.org/10.1029/2004GC000895.
Pfänder, J.A., Jochum, K.P., Kozakov, I., Kröner, A., Todt, W., 2002. Coupled evolution of back-arc and island arc-like mafic crust in the late-Neoproterozoic Agadagh Tes-Chem ophiolite, Central Asia: evidence from trace element and Sr-Nd-Pb isotope data. Contributions to Mineralogy and Petrology 143, 154–174.
Pilitsyna, A., Tretyakov, A.A., Degtyarev, K.E., Cuthbert, S.J., Batanova, V.G., Kovalchuk, E.V., 2018. Eclogites and garnet clinopyroxenites in the Anrakhai complex, Central Asian Orogenic Belt, Southern Kazakhstan: P-T evolution, protoliths and some geodynamic implications. Journal of Asian Earth Sciences 153, 325–345.
Plank, T., Langmuir, C.H., 1998. The chemical composition of subducting sediment and its consequences for the crust and mantle. Chemical Geology 145, 325–394.
Regelous, M., Hofmann, A.W., Abouchami, W., Galer, S.J.G., 2003. Geochemistry of lavas from the Emperor Seamounts, and the geochemical evolution of Hawaiian magmatism from 85 to 42 Ma. Journal of Petrology 44 (1), 113–140.
Robin, C., Colantoni, P., Gennesseaux, M., Rehault, J.P., 1987. Vavilov seamount: a mildly alkaline Quaternary volcano in the Tyrrhenian basin. Marine Geology 78, 125–136.
Ross, P.-S., Bedard, J.H., 2009. Magmatic affinity of modern and ancient subalkaline volcanic rocks determined from trace-element discriminant diagrams. Canadian Journal of Earth Sciences 46, 823–839.
Saccani, E., 2015. A new method of discriminating different types of post-Archean ophiolitic basalts and their tectonic significance using Th-Nb and Ce-Dy-Yb systematics. Geoscience Frontiers 6, 481–501.
Safonova, I., 2014. The Russian-Kazakh Altai orogen: an overview and main debatable issues. Geoscience Frontiers 5, 537–552.
Safonova, I., Kojima, S., Nakae, S., Romer, R., Seltmann, R., Sano, H., Onoue, T., 2015. Oceanic island basalts in accretionary complexes of SW Japan: Tectonic and petrogenetic implications. Journal of Asian Earth Sciences 113, 508–523.
Safonova, I., 2017. Juvenile versus recycled crust in the Central Asian Orogenic Belt: implications from ocean plate stratigraphy, blueschist belts and intra-oceanic arcs. Gondwana Research 47, 6–27.
Safonova, I., Maruyama, S., 2014. Asia: a frontier for a future supercontinent. International Geology Review 56, 1051–1071.
Safonova, I.Yu, Santosh, M., 2014. Accretionary complexes in the Asia-Pacific region: tracing archives of ocean plate stratigraphy and tracking mantle plumes. Gondwana Research 25, 126–158.
Safonova, I.Yu, Simonov, V.A., Buslov, M.M., Ota, T., Maruyama, Sh, 2008. Neoproterozoic basalts of the Paeo-Asian Ocean (Kurai accretionary zone, Gorny Altai, Russia): geochemistry, petrogenesis, and geodynamics. Russian Geology and Geophysics 49, 254–271.
Safonova, I.Yu, Buslov, M.M., Simonov, V.A., Izokh, A.E., Komiya, T., Kurganskaya, E.V., Ohno, T., 2011a. Geochemistry, petrogenesis and geodynamic origin of basalts from the Katun accretionary complex of Gorny Altai (southwestern Siberia). Russian Geology and Geophysics 52, 421–442.
Safonova, I.Yu, Sennikov, N.V., Komiya, T., Bychkova, Y.V., Kurganskaya, E.V., 2011b. Geochemical diversity in oceanic basalts hosted by Zasur'ya accretionary complex, NW Russian Altai, Central Asia: implications from trace elements and isotopes. Journal of Asian Earth Sciences 42, 191–207.
Safonova, I.Yu, Simonov, V.A., Kurganskaya, E.V., Obut, O.T., Romer, R.L., Seltmann, R., 2012. Late Paleozoic oceanic basalts hosted by the Char suture-shear zone, East Kazakhstan: geological position, geochemistry, petrogenesis and tectonic setting. Journal of Asian Earth Sciences 49, 20–39.
Safonova, I., Biske, G., Romer, R.L., Seltmann, R., Simonov, V., Maruyama, S., 2016. Middle Paleozoic mafic magmatism and ocean plate stratigraphy of the South Tianshan, Kyrgystan. Gondwana Research 30, 236–256.
Safonova, I., Kotlyarov, A., Krivonogov, S., Xiao, W., 2017. Intra-oceanic arcs of the Paleo-Asian Ocean. Gondwana Research 50, 167–194.
Safonova, I., Komiya, T., Romer, R.L., Simonov, V., Seltmann, R., Rudnev, S., Yamamoto, S., Sun, M., 2018a. Supra-subduction igneous formations of the Char ophiolite belt, East Kazakhstan. Gondwana Research 59, 159–179.
Safonova, I., Maruyama, S., Kotler, P., Perfilova, A., 2018b. Tectonic erosion at pacific-type convergent margins: evidence from the western central asian orogenic belt. In: Earth, Sea and Sky III: Proceedings of the International Joint Graduate Program Workshop in Earth and Environmental Sciences, p. 8.
Safonova, I., Obut, O., Savinskiy, I., Kotler, P., Khromykh, S., Krivonogov, S., Gurova, A., Perfilova, A., Chyormy, R., Petrenko, N., Maruyama, S., 2018c. The Itmurundy accretionary complex in northern Balkhash area: a Cambrian-Ordovician stage of the Paleo-Asian Ocean. In: Correlation of the Altaids and the Uralids: Deep Structure of the Lithosphere, Stratigraphy, Magmatism, Metamorphism Geodynamics and Metallogeny: Proceedings of the IV International Conference, Novosibirsk, April 2-6, 2018, pp. 130–132.
Salnikova, E.B., Kozakov, I.K., Kotov, A.B., Kroener, A., Todt, W., Bibikova, E.V., Nutman, A., Yakovleva, S.Z., Kovach, V.P., 2001. Age of palaeozoic granites and metamorphism in the tuvino-Mongolian massif of the central asian mobile belt: loss of precambrian microcontinent. Precambrian Research 110, 143–164.
Scholl, D.W., van Huene, R., 2007. Crustal recycling at modern subduction zones applied to the past — Issues of growth and preservation of continental basement crust, mantle geochemistry, and supersontinent reconstruction. Memoir of the Geological Society of America 200, 9–32. https://doi.org/10.1130/2007.1200(02).
Scott, R.B., Hajash Jr., A., 1976. Initial submarine alteration of basaltic pillow lavas: a microprobe study. American Journal of Science 276, 480–501.
Sdrolias, M., Müller, R.D., Mauffret, A., Bernardel, G., 2004. Enigmatic formation of the Norfolk Basin, SW Pacific: a plume influence on back-arc extension. Geochemistry, Geophysics, Geosystems 5 (6), Q06005. https://doi.org/10.1029/2003GC000643.
Sengör, A.M.C., Natal'in, B.A., Burtman, V.S., 1993. Evolution of the Altaid tectonic collage and Paleozoic crustal growth in Eurasia. Nature 364, 299–307.
Sengör, A.M.C., Natal'in, B.A., Sunal, G., van der Voo, R., 2018. The tectonics of the Altaids: crustal growth during the construction of the continental lithosphere of Central Asia between ~ 750 and ~ 130 Ma ago. Annual Review of Earth and Planetary Sciences 46, 439–494.
Seyfried, W.E., Berndt, M.E., Seewald, J.S., 1988. Hydrothermal alteration processes at mid-ocean ridges: constraints from diabase alteration experiments, hot-spring fluids and composition of the oceanic crust. The Canadian Mineralogist 26, 787–804.
Shen, P., Pan, H., Seitmuratova, E., Yuan, F., Jakupova, S., 2015. A Cambrian intra-oceanic subduction system in the Bozshakol area. Kazakhstan. Lithos 224–225, 61–77.
Shervais, J.W., 1982. Ti-V plots and the petrogenesis of modern and ophiolitic lavas. Earth and Planetary Science Letters 32, 114–120.
Sklyarov, E.V., Kovach, V.P., Kotov, A.B., Kuzmichev, A.B., Lavrenchuk, A.V., Perelyaev, V.I., Shchipansky, A.A., 2016. Boninites and ophiolites: problems of their relations and petrogenesis of boninites. Russian Geology and Geophysics 57, 127–140.
Song, S., Wang, M.-M., Xu, X., Wang, C., Niu, Y., Allen, M.B., Su, L., 2015. Ophiolites in the Xing'an-Inner Mongolia accretionary belt of the CAOB: implications for two cycles of seafloor spreading and accretionary orogenic events. Tectonics 34, 2221–2248. https://doi.org/10.1002/2015TC003948.
Staudigel, H., Hart, R., 1983. Alteration of basaltic glass: mechanism and significance for the oceanic crust-seawater budget. Geochimica et Cosmochimica Acta 47, 37–50.
Staudigel, H., Clague, D.A., 2010. The geological history of deep-sea volcanoes: biosphere, hydrosphere, and lithosphere interactions. Oceanography 23, 58–71.
Staudigel, H., Koppers, A.A.P., 2015. Seamounts and island building. In: Sigurdsson, H., Houghton, B., Rymer, H., Stix, J., McNutt, S. (Eds.), The Encyclopedia of Volcanoes, second ed., pp. 405–421.
Stern, R.J., Dickinson, W.R., 2010. The Gulf of Mexico is a backarc basin. Geosphere 6 (6), 739–754.
Stipska, P., Schulmann, K., Lehmann, J., Corsini, M., Lexa, O., Tomurhuu, D., 2010. Early Cambrian eclogites in SW Mongolia: evidence that the Palaeo-Asian Ocean suture extend further east than expected. Journal of Metamorphic Geology 28, 915–933.
Sun, M.-D., Xu, Y.-G., Wilde, S.A., Chen, H.L., Yang, S.-F., 2015. The permian Dongfanghong island arc gabbro of the wandashan orogen, NE China: implications for paleo-pacific subduction. Tectonophyics 659, 122–136.
Tararin, I.A., Lekikov, E.P., Werner, R., 2003. Petrology and geochemistry of the volcanic rocks dredged from Geophysicist Seamount in the Kurile Basin; Evidence for the existence of thinned continental crust. Gondwana Research 6 (4), 757–765.
Tatsumi, Y., Shukuno, H., Yoshikawa, M., Chang, Q., Sato, K., Lee, M.W., 2005. The petrology and geochemistry of volcanic rocks on Jeju island: plume magmatism along the Asian continental margin. Journal of Petrology 46, 523–553.
Tian, Z., Xiao, W., Windley, B.F., Lin, L., Han, C., Zhang, J., Wan, B., Ao, S., Song, D., Feng, J., 2014. Structure, age, and ectonic development of the Huoshishan-Niujuanzi ophiolitic mélange, Beishan, southernmost Altaids. Gondwana Research 25, 820–841.
Tripathi, S.K., Nagendran, G., Karthikeyan, M., Vasu, P., Tripathy, S.K., Varghese, S., Raghav, S., Resmi, S., 2017. Morphology of submarine volcanic seamounts from inner volcanic arc of Andaman Sea. Indian Journal of Geosciences 71 (3), 451–470.
Trua, T., Serri, G., Marani, M., Renzulli, A., Gamberi, F., 2002. Volcanological and petrological evolution of marsili seamount (southern tyrrhenian sea). Journal of Volcanology and Geothermal Research 114, 441–464.
Turkina, O.M., 2002. Tonalite-trondhjemite complexes of subduction-related settings (by the example of Late Riphean plagiogranitoids of the southwestern margin of the Siberian Platform). Russian Geology and Geophysics 43, 403–417.
Volkova, N.I., Budanov, V.I., 1999. Geochemical discrimination of metabasalt rocks of the Fan-Karategin transitional bkueschist/greenschist belt, South Tianshan, Tajikistan: seamount volcanism and accretionary tectonics. Lithos 47, 201–216.
Volkova, N.I., Sklyarov, E.V., 2007. High-pressure complexes of the central asian fold belt: geological setting, geochemistry, and geodynamic implications. Russian Geology and Geophysics 48, 109–119.
Volkova, N.I., Stupakov, S.I., Babin, G.A., Rudnev, S.N., Mongush, A.A., 2009. Mobility of trace elements during subduction metamorphism as exemplified by the blueschists of the Kurtushibinsky Range, Western Sayan. Ge4ochemistry International 47 (4), 380–392.
Von Huene, R., Scholl, D.W., 1991. Observations at convergent margins concerning sediment subduction, sediment erosion, and the growth of continental crust. Reviews of Geophysics 29, 279–316.
Volkova, N.L., Travin, A.V., Yudin, D.S., 2011. Ordovician blueschist metamorphism as a reflection of accretion-collision events in the Central Asian orogenic belt. Russian Geology and Geophysics 52, 72–84.

Wang, Z., Sun, S., Li, J., Hou, Q., Qin, K., Xiao, W., Hao, J., 2003. Paleozoic tectonic evolution of the northern Xinjiang, China: geochemical and geochronological constraints from the ophiolites. Tectonics 22 (2). https://doi.org/10.1029/2002TC001396.
Wang, B., Faure, M., Shu, L.S., de Jong, K., Charvet, J., Cluzel, D., Jahn, B.M., Chen, Y., Ruffet, G., 2010. Structural and geochronological study of High-Pressure metamorphic rocks in the Kekesu section (Northwestern China): implications for the late Paleozoic tectonics of the southern Tianshan. The Journal of Geology 118, 59–77.
Wang, B., Shu, L., Faure, M., Jahn, B-m., Cluzel, D., Charvet, J., Chung, S-l., Meffre, S., 2011. Paleozoic tectonics of the southern Chinese Tianshan: insights from structural, chronological and geochemical studies of the Heiyingshan ophiolitic mélange (NW China). Tectonophysics 497, 85–104.
Wang, J-y., Yang, Y-c., Huang, Y-w., Hou, Y-s., Tan, Y., Xhang, G-b., 2016. Formation ages and tectonic significance of ophiolites in wandashan terrane of the eastern Heilongjiang. Journal of Earth Sciences and Environment 38 (2), 182–195.
Windley, B.F., Alexeiev, D., Xiao, W., Kröner, A., Badarch, G., 2007. Tectonic models for accretion of the central asian orogenic belt. Journal of the Geological Society, London 164, 31–47.
Winchester, J.A., Floyd, P.A., 1977. Geochemical discrimination of different magma series and their differentiation products using immobile elements. Chemical Geology 20, 323–343.
Wong, K., Sun, M., Zhao, G., Yuan, C., Xiao, W., 2010. Geochemical and geochronological studies of the Alegedayi Ophiolitic complex and its implications for the evolution of the Chinese Altai. Gondwana Research 18, 438–454.
Xiao, W.J., Huang, B.C., Han, C.M., Sun, S., Li, J.L., 2010. A review of the western part of the Altaids: a key to understanding the architecture of accretionary orogens. Gondwana Research 18, 253–273.
Xiao, W., Han, C., Liu, W., Wan, B., Zhang, J., Ao, S., Zhang, Z., Song, D., Tian, Z., Luo, J., 2014. How many sutures in the southern central asian orogenic belt: insights from east xinjiang – west ganso (NW China)? Geoscience Frontiers 5, 525–536.
Yamamoto, S., Senshu, H., Rino, S., Omori, S., Maruyama, S., 2009. Granite subduction: Arc subduction, tectonic erosion and sediment subduction. Gondwana Research 15, 443–453.
Yan, Q., Castillo, P.R., Shi, X., 2012. Geochemistry of basaltic lavas from the southern Lau Basin: input of compositionally variable subduction components. International Geology Review 54 (12), 1456–1474.
Yang, G., Li, Y., Santosh, M., Gu, P., Yang, B., Zhang, B., Wang, H., Zhong, X., Tong, L., 2012a. A neoproterozoic seamount in the paleoasian ocean: evidence from zircon U-Pb geochronology and geochemistry of the mayile ophiolitic mélange in west junggar, NW China. Lithos 140–141, 53–65.
Yang, G., Li, Y., Gu, P., Tong, B., Zhang, H., 2012b. Geochronological and geochemical study of the darbut ophiolite complex in the West junggar (NW China): implications for the petrogenesis and tectonic evolution. Gondwana Research 21, 1037–1049.
Yang, G., Li, Y., Santosh, M., Yang, B., Yan, J., Zhang, B., Tong, L., 2012c. Geochronology and geochemistry of basaltic rocks from the Sartuohai ophiolitic mélange, NW China: implications for a Devonian mantle plume within the Junggar Ocean. Journal of Asian Earth Sciences 59, 141–155.
Yarmolyuk, V.V., Kovalenko, V.I., Kozlovsky, A.M., Kovach, V.P., Sal'nikova, E.B., Kovalenko, D.V., Kotov, A.B., Kudryashova, E.A., Lebedev, V.I., Eenzhin, G., 2008. Crust-forming processes in the hercynides of the central asian foldbelt. Petrology 16 (7), 679–709.
Ye, X.T., Zhang, C.-L., Zou, H.-B., Yao, C.-Y., Dong, Y.-G., 2017. Age and geochemistry of the Zhaheba ophiolite complex in eastern Junggar of the Central Asian Orogenic Belt (CAOB): implications for the accretion process of the Junggar terrane. Geological Magazine 154, 419–440.
Zhang, Z., Zhou, G., Kusky, T.M., Yan, S., Chen, B., Zhao, L., 2009. Late Paleozoic volcanic record of the Eastern Junggar terrane, Xinjiang, Northwestern China: major and trace element characteristics, Sr-Nd isotopic systematics and implications for tectonic evolution. Gondwana Research 16, 201–215.
Zhang, Z., Li, H., Li, J., Tang, W., Chen, Y., Luo, Z., 2015. Geochronology and geochemistry of the eastern Erenhot ophiolitic complex: implications for the tectonic evolutionof the inner Mongolia-daxinganling orogenic belt. Journal of Asian Earth Sciences 97, 279–293.
Zhang, P., Wang, G., Polat, A., Shen, T., Chen, Y., Zhu, C., Wu, G., 2018a. Geochemistry of mafic rocks and cherts in the Darbut and Karamay ophiolitic mélanges in West Junggar, northwest China: evidence for a Late Silurian to Devonian back-arc basin system. Tectonophysics 745, 395–411.
Zhang, P., Wang, G., Polat, A., Zhu, C., Shen, T., Chen, Y., Chen, C., Guo, J., Wu, G., Liu, Y., 2018b. Emplacement of the ophiolitic melanges in the west Karamay area: implications for the Late Paleozoic tectonic evolution of Wesr Junggar, northwestern China. Tectonophysics 747–748, 259–280.
Zhang, L., Chu, X., Zhang, L., Fu, B., Bader, T., Du, J., Li, X., 2018c. The early exhumation history of the Western Tianshan UHP metamorphic belt, China: new constraints from titanite U-Pb geochronology and thermobarometry. Journal of Metmorphic Geology 36 (5), 631–651. https://doi.org/10.1111/jmg.12422.
Zhao, P., Chen, Y., Xu, B., Faure, M., Shi, G., Choulet, F., 2013. Did the Paleo-Asian Ocean between North China block and Mongolia block exist during the late paleozoic? First paleomagnetic evidence from central-eastern inner Mongolia, China. Journal of Geophysical Research, Solid Earth 118, 1873–1894.
Zhao, L., He, G., 2014. Geochronology and geochemistry of the Cambrian (~518 Ma) Chagantaolegai ophiolite in northern West Junggar (NW China): constraints on spatiotemporal characteristics of the Chingiz-Tarbagatai megazone. International Geology Review 56 (10), 1181-1181.
Zheng, R., Wu, T., Zhang, W., Xu, C., Meng, Q., 2013. Late paleozoic subduction system in the southern central asian orogenic belt: evidences from geochronology and geochemistry of the xiaohuangshan ophiolite in the beishan orogenic belt. Journal of Asian Earth Sciences 62, 463–475.
Zhou, J.-B., Wilde, S.A., Zhang, X.-Z., Zhao, G.-C., Zheng, C.-Q., Wang, Y.-J., Zhang, X.-H., 2009. The onset of Pacific margin accretion in NE China: evidence from the Heilongjiang high-pressure metamorphic belt. Tectonophysics 478, 230–246.
Zhou, J.-B., Wilde, S.A., 2013. The crustal accretion history and tectonic evolution of the NE China segment of the Central Asian Orogenic Belt. Gondwana Research 23, 1365–1377.
Zhou, J.-B., Cao, J.-L., Wilde, S.A., Zhao, G.-C., Zhang, J.-J., Wang, S., 2014. Paleo-Pacific subduction-accretion: evidence from geochemical and U-Pb zircon dating of the Nadanhada accretionary complex, NE China. Tectonics 33, 2444–2466. https://doi.org/10.1002/2014TC003637.
Zhu, M., Miao, L., Baatar, M., Zhang, F., Anaad, C., Yang, S., Li, Y., 2014a. Zircon ages and geochemical data of the Biluutiin ovoo ophiolite: implication for the tectonic evolution of South Mongolia. International Geology Review 56 (14), 1769–1782.
Zhu, M., Baatar, M., Miao, L., Anaad, C., Zhang, F., Yang, S., Li, Y., 2014b. Zircon ages and geochemical compositions of the Manlay ophiolite and coeval island arc: implications for the tectonic evolution of South Mongolia. Journal of Asian Earth Sciences 96, 108–122.
Zhu, Y., Chen, B., Qiu, T., 2015. Geology and geochemistry of the Baijiantan-Baikouquan ophiolitic mélanges: implications for geological evolution of west Junggar, Xinjiang, NW China. Geological Magazine 152 (1), 41–69.
Zhu, M.-S., Zhang, F., Miao, L.-C., Baatar, M., Abaad, C., Yang, S.-H., Li, X.-B., 2017. The late carboniferous khuhu davaa ophiolite in northeastern Mongolia: implications for the tectonic evolution of the mongol-okhotsk ocean. Geological Journal 1–16. https:/doi.org/10.1002/gj.2955.
Zonenshain, L.P., Kuzmin, M.I., Natapov, L.M., 1990. Geology of the USSR: A Plate-Tectonic Synthesis, vol. 21. American Geophysical Union, Geodynamic Series.

**Harald Furnes** became a full professor at the Department of Earth Science, University of Bergen, Norway, in 1985, and since 2014 an Emeritus professor at the same institute. He received his D.Phil. at Oxford University, UK, in 1978. His main research interests have been connected to magmatic and volcanic rocks. This involves physical volcanology, geochemistry and petrology, mainly related to ophiolites and island arc development of various ages, as well as Precambrian greenstones. In particular the Paleoarchean Barberton Greenstone Belt has been one of the main research issues. Another research focus has been related to the alteration of volcanic glass, which again led to a long-term study on the interaction between submarine basaltic volcanic rocks and micro-organisms, and the search for traces of early life. On these topics he has given numerous talks at national and international conferences and published a number of refereed papers in international journals.

**Inna Safonova** is a Senior Research Scientist at the Sobolev Institute of Geology and Mineralogy SB RAS and the Head of the Laboratory of Evolution of Paleo-Oceans and Mantle Magmatism (LEPOM) at the Geology-Geophysical Department of the Novosibirsk State University, both in Novosibirsk, Russia. She received her M.Sc. (1987) from the Novosibirsk State University (Honors), and her Ph.D. (2005) from the Russian Academy of Sciences. She has been a visiting researcher in the Tokyo Institute of Technology (2004–2015), University of Tokyo (2010–2014) and a Brain Pool Program Researcher in the Korea Institute of Geology and Mineral Resources (2010–2012). Awardee of the Japan Society for Promotion of Science in 2007–2009, 2014–2015 and 2017. Inna has published over 90 peer-reviewed papers in SCI journals; Associate editor of *Gondwana Research*, *Geoscience Frontiers* and *Journal of Asian Earth Sciences*. Research fields include Pacific-type orogenic belts, continental growth in Central Asia, ocean plate stratigraphy, tectonic erosion, geochronology, igneous geochemistry and petrology, mantle magmatism. Proposer and Leader of IGCP#592 Project "Continental construction in Central Asia" of UNESCO-IUGS (2012–2016). Leader of a Megagrant Project of the Ministry of Education and Science of Russia "A multidisciplinary study of Pacific-type orogenic belts and development of a holistic model linking evolution of oceans, their active margins and mantle magmatism" (No. 14.Y26.31.0018; 2017–2019).